DIRECT CO_2 CAPTURE FROM AMBIENT AIR WITH AMINE FUNCTIONALIZED SILICA AND CELLULOSE MATERIALS

A Thesis
Presented to
The Academic Faculty

by

Chunjae Yoo

In Partial Fulfillment
of the Requirements for the Degree
Master of Science in Paper Science Engineering from the
School of Chemical and Biomolecular Engineering

Georgia Institute of Technology

DECEMBER, 2015

COPYRIGHT© 2015 BY CHUNJAE YOO

DIRECT CO_2 CAPTURE FROM AMBIENT AIR WITH AMINE FUNCTIONALIZED SILICA AND CELLULOSE MATERIALS

Approved by:

Dr. Christopher W. Jones, Advisor
School of Chemical & Biomolecular Engineering
Georgia Institute of Technology

Dr. Yulin Deng
School of Chemical & Biomolecular Engineering
Georgia Institute of Technology

Dr. Ryan P. Lively
School of Chemical & Biomolecular Engineering
Georgia Institute of Technology

Date Approved: November 05, 2015

ACKNOWLEDGEMENTS

First of all, I would like to thank my adviser, Dr. Jones, for supporting my research. Whenever I encountered barriers, he did not force me to follow his directions. He just provided possible options and their possibilities of success, which made me understand the situation correctly and escape from the barriers or problems in a short time. Under his guidance, I could successfully finish my MS degree. I truly appreciate his time and advice he gave me.

I also would like to thank my group members. Even though Jones group consists of various and distinct personalities, they are acting like one team with dedicative and cooperative attitude. These atmosphere helps me adapt myself to new circumstance and develop my research based on the inter-subgroup collaborations.

Lastly, I would like to thank my family and friends for encouraging me to go forward.

TABLE OF CONTENTS

LIST OF TABLES

LIST OF FIGURES

SUMMARY

In chapter 1, the crisis that human beings will face in the near future was covered by comparing the historical atmospheric CO_2 concentration for the last 800,000 years with the present high CO_2 concentration (400 ppm). Since the atmospheric CO_2 concentration is in close association with global temperature and sea level, with current CO_2 emission levels, the global temperature and sea level will keep increasing. According to the current CO_2 emissions by sectors, almost half of emitted CO_2 could be captured by direct air capture and another half of CO_2 are released from flue gas sources. Thus, research on direct air capture as well as flue gas capture are necessary to effectively control the increasing CO_2 concentration. Considering an industrial application for direct CO_2 capture from air, amine containing solid adsorbents were proposed as promising materials. In addition to the use of conventional inorganic support materials, a biodegradable cellulose support was also studied.

In chapter 2, to better understand CO_2 adsorption on amine containing silica adsorbents, a molecular approach to adsorbent design was introduced. A mesoporous silica SBA15 was modified with an array of amine-containing organosilanes including (i) propyl-amine, $SiCH_2CH_2CH_2NH_2$ (MONO), (ii) propyl-ethylenediamine, $SiCH_2CH_2CH_2NHCH_2CH_2NH_2$ (DI), (iii) propyl-diethylenetriamine, $SiCH_2CH_2CH_2NHCH_2CH_2NHCH_2CH_2NH_2$ (TRI), and (iv) propyl-triethylenetetramine, $SiCH_2CH_2CH_2NHCH_2CH_2N(CH_2CH_2NH_2)_2$ (TREN) and the low loading silane adsorbents (~0.45 mmol silane/g) were evaluated for their CO_2 adsorption properties, with a focus on gaining insight into the propensity for intramolecular vs. intermolecular CO_2 adsorption. Adsorption isotherms at low CO_2 coverages were measured while simultaneously recording the heat evolved via a Tian-Calvet calorimeter. The results was compared on a silane molecule

efficiency basis (mol CO_2 adsorbed / mol silane), to assess the potential for intramolecular CO_2 adsorption, employing two amine groups in a single silane molecule. As the number of amines in the silane molecule increased (MONO<DI<TREN~TRI), the silane molecule efficiency was enhanced owing to the ability to intramolecularly capture CO_2. Analysis of the CO_2 uptake for samples with the surface silanols removed by capping demonstrated that cooperative uptake due to amine-CO_2-silanol interactions was also possible over these adsorbents, and was the primary mode of sorption for the MONO material at the studied low silane loading. As the propensity for intramolecular CO_2 capture increased due to the presence of multiple amines in a single silane molecule (MONO<DI<TREN~TRI), the measured heat of adsorption also increased. This study of various amine-containing silanes at low coverage was the first to provide significant, direct evidence for intramolecular CO_2 capture in a single silane molecule. Furthermore, it provided evidence for the relative heats of adsorption for physisorption on a silanol laden surface (ca. 37 kJ/mol), a silanol capped surface (ca. 25 kJ/mol), via amine-CO_2-silanol interactions (ca. 46 kJ/mol), and via amine-CO_2-amine interactions at low surface coverages (ca. 65 kJ/mol).

In chapter 3, the potential performance of microfibrillated cellulose (MFC) was evaluated as a biodegradable support for amine based CO_2 adsorption. Because of the different physical and chemical properties of MFC with common inorganic supports (metal oxide), water was used as a solvent for impregnation or grafting of amine containing molecules. As an application of class 1 materials, PEI or TREN was impregnated onto the MFC and the CO_2 capacities were compared with materials made from the same amount of amine impregnated on porous silica. While PEI40/MFCs showed slightly lower CO_2 uptake and amine efficiencies than PEI40/SBA15, TREN40/MFCs did not adsorb CO_2 at all. In contrast, TREN40/SBA15 had a similar amine efficiency with PEI40/MFC. From the SEM image analysis, extremely thickened

fibers (30 μm diameter) for TREN40/MFC were observed, with the fibers of PEI40/MFC only somewhat agglomerated with an overall structure similar to the bare MFC. Considering the fiber structure of the PEI/MFC and TREN/MFC adsorbents, the primary amines of TREN are suggested to participate in hydrogen bonding with hydroxyl groups of MFC; thus, TREN was likely located between the fibers, and consequently, the MFCs stick together and assemble into thick fibers after freeze drying. However, since PEI has a highly branched structure, even though the outer primary amines of PEI might be connected to hydroxyl groups of MFC via hydrogen bonding, the fibers of MFC remain relatively isolated and maintain their structure. In the case of class 2 materials, various amounts of two different silanes, 3-aminopropyltriethoxysilane (APTES) and 3-aminopropyldiethylmethylsilane (APDES), were grafted on the MFC. The CO_2 uptake for APDES adsorbents increased with silane loadings and maximized (0.85 mmol CO_2/g) when 10 mmol of silane was grafted on 1 g of MFC, whereas APTES adsorbents showed very low CO_2 uptakes. During the grafting process in aqueous MFC slurries, APDES was polymerized into a linear structure and APTES was polymerized in a 3D structure, as verified with solid state ^{29}Si NMR and FTIR analysis. The chemically adsorbed CO_2 species (alkyl ammonium carbamates) on APDES10/MFC were verified by *in-situ* FTIR analysis. From SEM analysis, relatively uniform pore filling was observed with APDES/MFCs with increasing silane loadings, but lumped bulk poly(siloxane) structures were observed from APTES/MFCs, which indicated that APTES was not uniformly grafted on the surface of MFC. Consequently, it was suggested that the number of alkoxy groups in the silane molecule caused the distinguishably different structures after polymerization in water and the final structures on the MFC affected CO_2 capacities.

CHAPTER 1

INTRODUCTION

1.1. The Necessity of CO_2 capture

Since our environmental systems are maintained with interactions between living organisms and nonlinving components, small changes in one part of an ecosystem can influence others parts of the world. These influences can lead to unexpected chain reactions that ripple across the natural environment. Such changes evolved from natural occurrences have appeared periodically over the millennia. From this context, natural phenomenon such as repetitions of glacial–interglacial eras or seasons can be explained. However, recently, there has been a tremendous amount of inflow of anthropologic products into the natural system, which may alter or break down these natural cycles. The quality of life for human beings has become highly developed since the industrial revolution of ca. 1760, but under the indiscriminate development that has ensued, the environment has ironically been significantly harmed, which undoubtedly will alter the quality of the human condition for future generations. As one indicator of the effects of human development on the global ecosystem, the atmospheric CO_2 concentration has substantially increased over the last century and the current level has reached 400 parts per million (ppm). Based on the history of the atmospheric CO_2 concentration for the last 800,000 years (before 1950), the CO_2 concentration has never been above the 300 ppm level. During the last 800,000 years, the atmospheric CO_2 concentration had fluctuated from 170 ppm to 300 ppm, and these trends affected the global temperature trend, as shown in Figure 1.1.

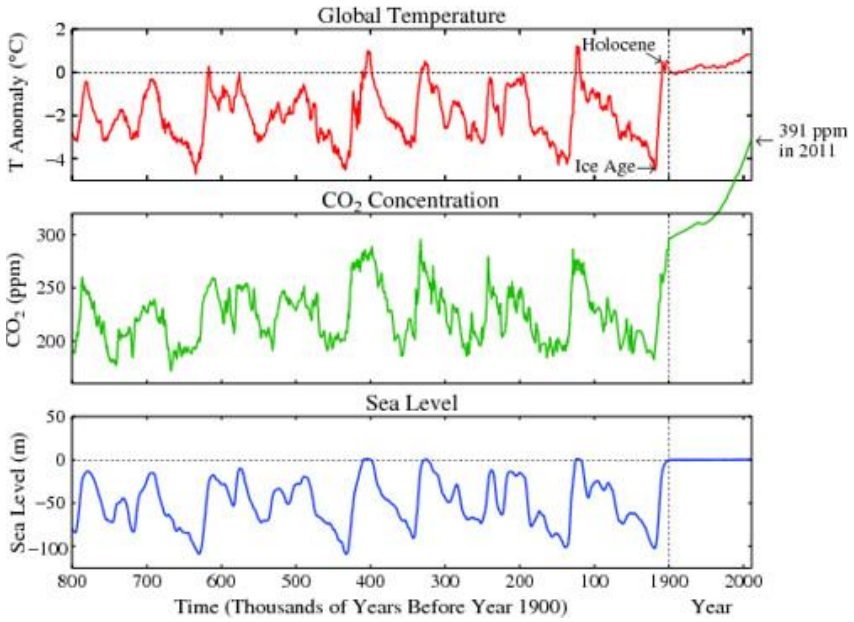

Figure 1.1. History of global temperature, CO_2 concentration and sea level for 800,000 years.[1]

The global temperature has shown almost exactly the same trend as the atmospheric CO_2 concentration because CO_2 is a major greenhouse gas. When the CO_2 concentration increased, the global temperature also increased, and we have called this period interglacial, whereas when the CO_2 concentration was near a minimum, glacial eras were started. As stated above, the global ecosystem had been harmonized for a long time, and the atmospheric CO_2 concentration was maintained under the 300 ppm upper limit observed for the last 800,000 years. With global industrialization increasing since 1760, the atmospheric CO_2 concentration has increased and under the circumstances where sustainable development is not widely considered, the CO_2 level is expected to keep increasing. In addition to the increasing global temperature, the sea level is also affected by the atmospheric CO_2 concentration. These factors are intimately connected to each other so their changing trends are also similar. As the sea level increases, global lowlands are about to become submerged. Under the situation that the environmental recovery capacity was overwhelmed, the Intergovernmental Panel on Climate Change (IPCC) reported in a Special

Report on Emissions Scenarios (SRES), that the atmospheric CO_2 concentration in the year 2100 will be between 540 and 970 ppm, based on several key scenarios.[2]

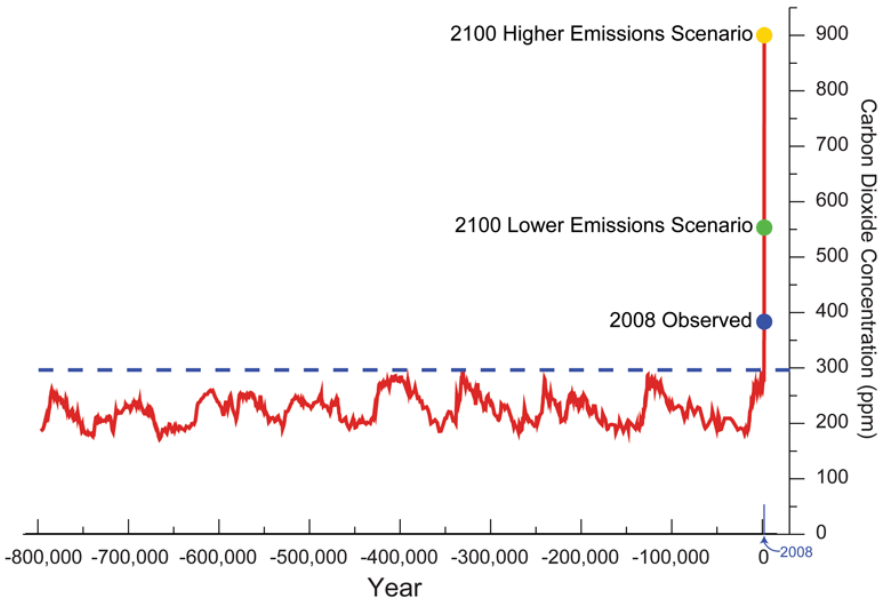

Figure 1.2. Estimated CO_2 concentration in 2100 based on the emission scenarios of the IPCC.[2]

1.2. Feasibility of direct air capture (DAC) of CO_2

To maintain CO_2 concentrations near the current levels, DAC technologies need to be developed in parallel with flue gas capture approaches. Considering the sources of the world's CO_2 emissions, the two largest sources are from energy supply (31 %) and industry (21 %).[3] The CO_2 emissions from these two sources are called flue gas in this work, being produced via hydrocarbon combustion, having CO_2 concentrations in the range of 10-15%. To reduce the CO_2 emissions from these sources, post or pre combustion CO_2 capture processes have been researched for over a decade. The CO_2 emitting facilities related to energy supply and industry are localized in specific areas or at key "point sources" and are associated with high CO_2 outflows at moderate concentrations (10-15 %) in flue gas. At these point sources, CO_2 capture is being conducted

effectively using various type of CO_2 adsorption or absorption technologies. However, other than these point sources, another almost 50 % of CO_2 emissions cannot be effectively managed by these techniques. The remaining sources (transport 27 %, residential and commercial buildings 12 %, and agriculture 9 %) are widely dispersed all over the world and the expelled concentrations of CO_2 are generally quite low compared to flue gas. For these reasons, applying the same technology used for flue gas capture has significant limitations for the capture of dilute CO_2 from these sources.

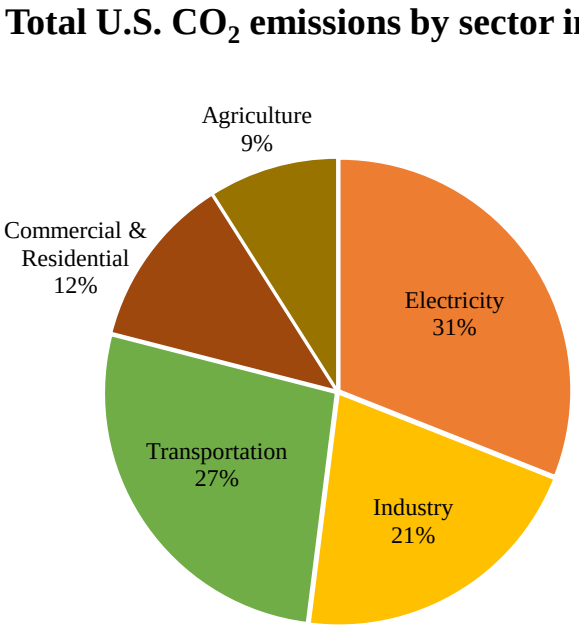

Figure 1.3. Total U.S. CO_2 emission by sector in 2013.[3]

However, if we can develop new adsorbents and processes for DAC technologies, the increasing CO_2 concentration can be effectively controlled DAC technologies which are important for a variety of reasons. First, they can adsorb mobile CO_2 emissions from automobiles, ships and aircraft. In addition, DAC technology might reduce the complexity for carbon capture and storage (CCS) businesses. Currently, the captured CO_2 from flue gases need to be transported to appropriate sequestration facilities, where the CO_2 can be safely injected underground. Because of a geological limitations and regional conflicts over CO_2 storage sites, these facilities can often not

be developed near the emission sources, which causes rising transportation costs in the form of CO_2 pipelines. However, DAC technology can be located anywhere, since the air is a nearly uniform CO_2 source, and creation of DAC facilities near the storage site could alleviate this problem. Furthermore DAC can compensate for possible leakage of CO_2 from CCS sites. Even though, leak rate of stored CO_2 from storage site might be not that high, when considering that there is no method to re-capture the leaked CO_2, DAC might be a suitable method.

To support the feasibility and competitiveness of DAC for CO_2 management alternative approaches for moving the air (wind might be an alternative source) and alternative processes for sorption and regeneration of adsorbents are needed. However, because of the relative lack of experimental studies on DAC systems, scaling up to pilot scale for DAC is also a current constraint. Thus, increased research for DAC is required to actualize the potential advantages of DAC, as stated above.

1.3. Amine functionalized solid sorbents

The typical CO_2 concentration from post-combustion capture process is 300 times higher than that of DAC processes and CO_2 removal rate is about three times faster than for DAC processes. Thus, massive air flows through CO_2 sorbents would be necessary for economical DAC. On top of that, the electricity demand for DAC includes fan power to move air, which is proportional to the pressure drop through the gas-solid contactor.

Considering these operation conditions, amine functionalized solid adsorbents are suggested to be a promising material for capture of dilute CO_2. Amine functionalized adsorbents have attracted attention as useful materials for CO_2 adsorption.[4,5] A wide array of amine-containing molecules and macromolecules containing various types of amines (primary, secondary, tertiary

and combinations thereof) have been investigated for CO_2 adsorption in combination with numerous solid supports. Previously, we and others have categorized these adsorbents into three classes in accordance with their physical and chemical features.[6,7] In general, class 1 materials are classified as adsorbents containing amine molecules physically impregnated into the pores of a solid support. An array of amines, including those with short alkyl chains (e.g. diethylenetriamine (DETA)[8] and tetraethylenepentamine (TEPA)[9]) and branched polymers (e.g. poly(ethylenimine) (PEI)[10]) have been impregnated into porous support materials. Class 2 materials are based on the amine containing molecules that can be chemically grafted onto the support materials or are otherwise bound to the adsorbent via covalent bonds. Most commonly, amine-containing alkoxysilanes (e.g. aminopropyltrialkoxysilane[11], 3-(2-aminoethylamino)propyltrimethoxy silane[12] and 3-[2-(2-aminoethylamino)ethylamino]propyltrimethoxysilane[13] are grafted to pre-synthesized oxide supports or are co-condensed[14] with silica forming molecules such as tetraethylorthosilicate. Class 3 materials are synthesized by in-situ polymerization reactions of amine monomers (e.g. aziridine,[15] melamin,[16] L-lysine N-carboxyanhydride[17]) in the pores of support materials.

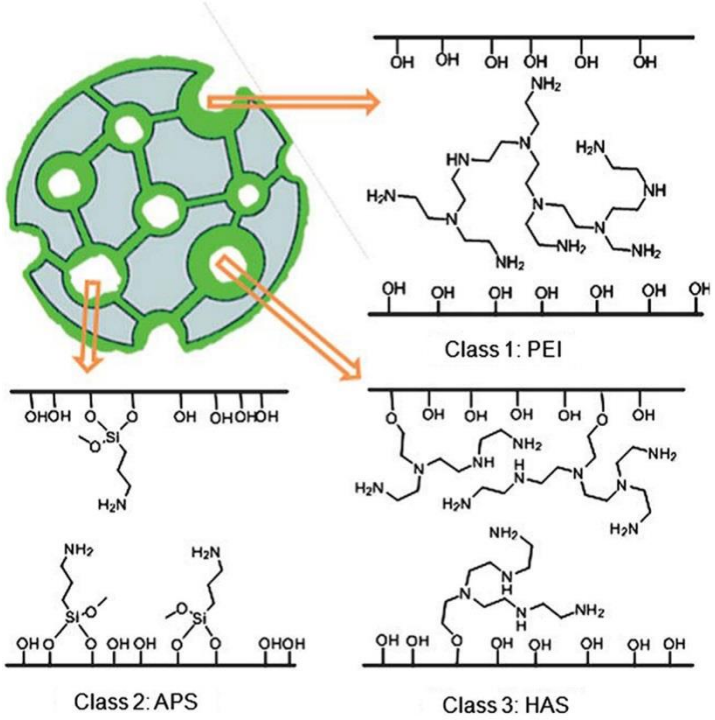

Figure 1.4. Categories of amine containing solid adsorbents.[6]

1.4. Nanocellulose

Since the early 2000s, nanocellulose materials have attracted attention as biodegradable structural materials because of their strong mechanical properties and compatibility with other materials after chemical modification. In general, plants consist of cellulose, hemicellulose and lignin. Among these components, cellulose accounts for 40-50 % of the composition and hemicellulose and lignin take up 25-35% and 15-20% respectively. From the organic composition view, cellulose is a high molecular weight linear polymer consisting of thousands of β-linked D-glucose units. However, it has secondary structure as well, as cellulose is a bundle of several building units.

As shown in Figure 1.5, elementary cellulose chain fibrils are packed into microfibrilllated cellulose and these units are assembled into larger cellulosic fibers.[18] This microfibrillated

cellulose can be obtained by mechanical[19–22] treatments or synthesized by specific bacteria (BC). (c.a. *Gluconacetobacter xylinus*[23]). Even though the microfibrillated cellulose (MFC) was first introduced in 1983 by Turbak et al[19], this material has not been widely researched because of the high energy consumption required for its synthesis. According to the energy consumption estimation from Eriksen et al.,[24] a mechanical treatment process using a homogenizer, microfluidizer, or grinder consumes about 70,000kwh/ton. To reduce the massive energy consumption for nanocellulose production, various research studied on enzymatic[25,26] or chemical[27] treatments to be used before the mechanical treatment have been conducted so that the cellulose fibers can be easily disintegrated by a less energy intensive process.

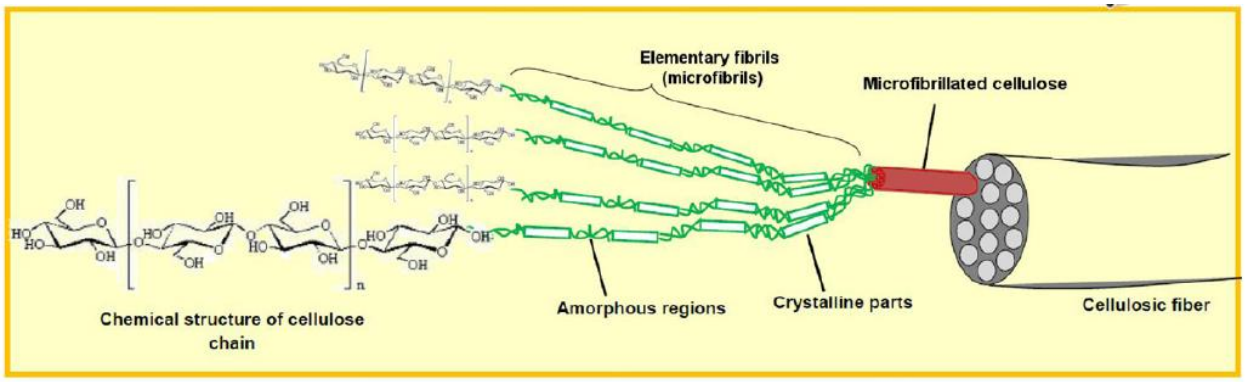

Figure 1.5. Details of the cellulosic fiber structure.[18]

The type, dimensions, synthesis method and TEM images of different forms of nanocellulose are summarized in Table 1.1.[28] As stated above, MFC can be obtained by delamination of wood pulp by mechanical treatment. Thus MFC has a high aspect ratio, 20-70 nm of diameter and several μm of length. MFC typically consists of amorphous and crystalline regions. Under the acid treatment, the amorphous regions of MFCs are hydrolyzed and only crystalline regions are retained, which are called nanocrystaline cellulose (NCC). Thus, the NCC has a similar

diameter as MFC but it has a shorter length (100-250 nm). While the MFC and NCC are synthesized from bulk cellulose fibers, bacteria cellulose is secreted by bacteria, thus it shows a narrow distribution of diameter (20-30 nm) and is several μm in length.

Table 1.1. Dimensions, synthesis process and TEM images of different nanocelluloses.[28]

Nanocellulose	Dimension	Synthesis process	TEM image
Microfibrillated cellulose (MFC)	Diameter: 20-70nm Length : several μm	Delamination of wood pulp by mechanical pressure	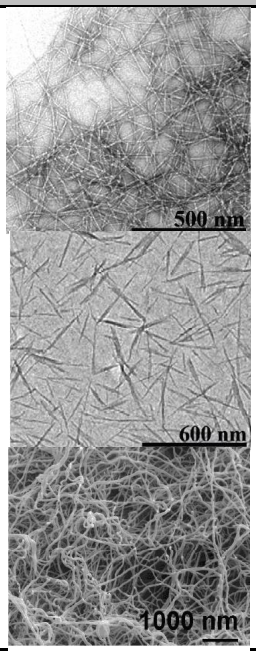
Nanocrystalline cellulose (NCC)	Diameter : 20-70 nm Length : 100-250 nm	Acid hydrolysis of cellulose	
Bacteria nanocellulose (BC)	Diameter : 20-30 nm	Bacterial synthesis	

Every glucose unit contains three hydroxyl groups on C2, C3 and C6. Ho et al.[29] estimated a density of hydroxyl groups of nanocellulose fibers under an assumption that only exposed hydroxyl groups of the outer surface of the fiber could participate in a modification reaction; thus, the diameter of the cellulose significantly affected the surface density of hydroxyl groups. When the diameter of the fiber was assumed to be 10 nm, the exposed density of hydroxyl groups was calculated as 4.2 OH mmol/g. However, this value decreased to 0.56 OH mmol/g when the diameter of fiber was 100 nm. Using these hydroxyl groups of nanocellulose, the material can be chemically modified to include other functional groups, as shown as Figure 1.6.[30]

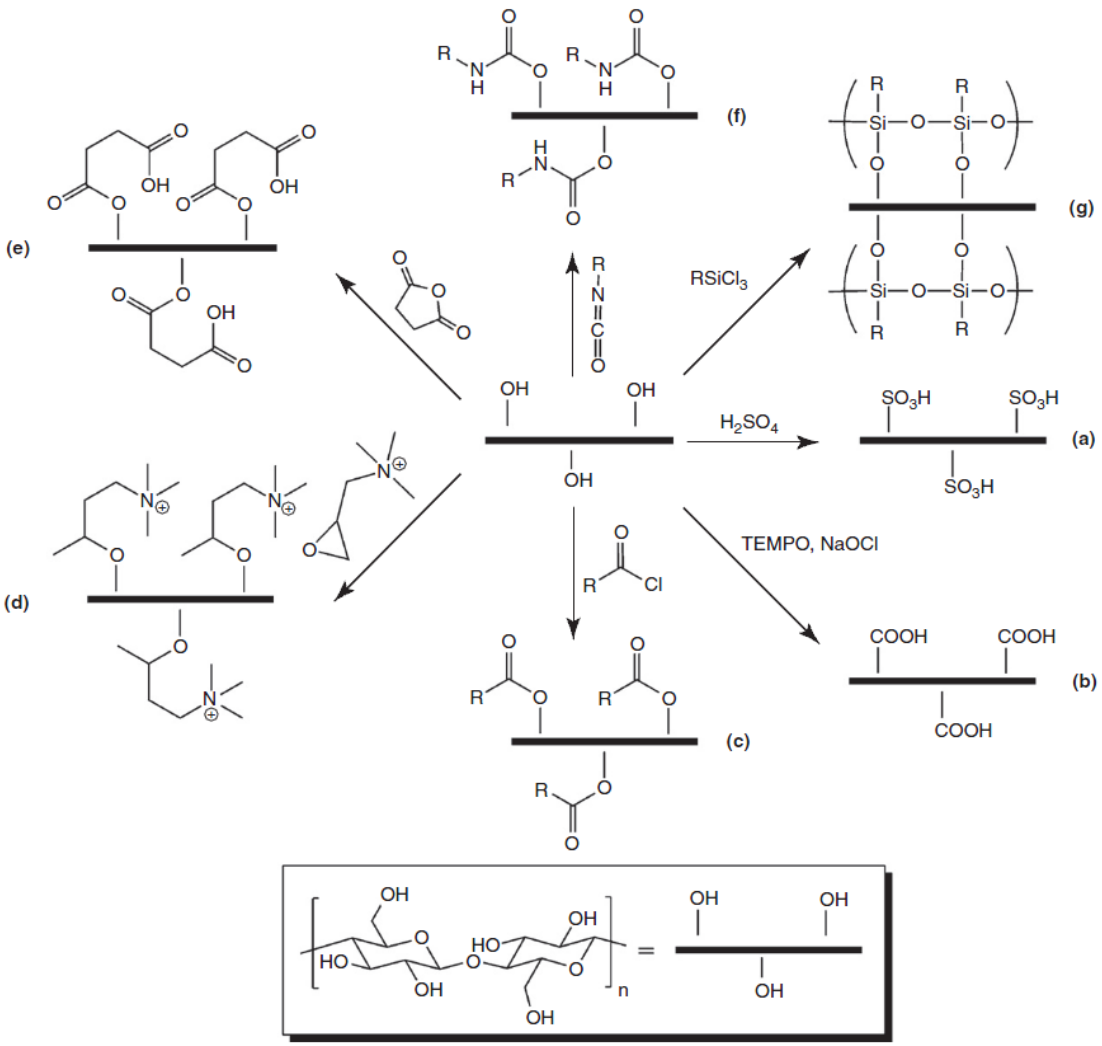

Figure 1.6. Probable chemical modifications at hydroxyl groups of nanocellulose.[30]

1.5. CO_2 adsorption mechanism with amine containing solid adsorbents

Based primarily on a range of *in-situ* FTIR studies of adsorbents contacted with CO_2,[31–34] the primary adsorbed species on supported amines have been identified as alkyl carbamic acid and alkylammonium carbamate species under both dry and humid conditions. Caplow[35] suggested the mechanism of formation of these species based on solution studies, involving a zwitterionic

mechanism, which requires free bases such as hydroxyl groups, water or another amine (1→2b, below).

$$RNH_2 + CO_2 \rightarrow RNH_2^+COO^- \quad (1)$$

$$RNH_2^+COO^- \rightarrow RNHCOOH \quad (2a)$$

$$RNH_2{}^+COO^- \text{ or } (RNHCOOH) + B \rightarrow RNHCOO^- + BH^+ \quad (2b)$$

where B and R is base and alkyl group, respectively.

However, studies utilizing *in-situ* IR spectroscopy and NMR spectroscopy have also identified carbamic acid species on the surface.[36] These may results from the pathway 1 to 2a shown above, with carbamic acid being a metastable species, or an intermediate on the way to alkyl ammonium carbamates (1→2a→2b). Some prior reports have suggested that carbamic acid species may be stabilized by free silanols on the silica surface.[37,38] Given these proposed sorption pathways, under dry conditions in the absence of water or hydroxide, two amines are required to adsorb one CO_2 molecule as an alkylammonium carbamate via amine-amine interactions, or one amine may capture one CO_2 molecule as a presumably less stable carbamic acid species.

1.6. Conclusions

The amine functionalized solid adsorbents have been considered as suitable materials for direct CO_2 capture from ambient air. Thus, various sorts of amine containing molecules and mesoporous supports have been studied to increase CO_2 adsorption capacities, and consequently, noticeable improvements in CO_2 uptake have been achieved and the framework of CO_2 capture with solid adsorbents has been established. However, the collected research to date has been

insufficient to understand CO_2 capture phenomenon on the molecular level. Based on fundamental research aimed at the mechanisms, kinetics, and thermodynamics of CO_2 adsorption with amine containing solid adsorbents, realization of practical approaches for direct CO_2 capture from air will be accelerated. From the same context, it is expected that the results from chapter 2, focusing on molecular level aspects of amine-CO_2 binding, would support key hypotheses that have not been verified quantitatively at the molecular level. In addition to the molecular approach, a new bio degradable support material, nanocellulose, will be introduced in chapter 3. From the view of its strong mechanical properties and potential for chemical modification, nanocellulose may be a promising sustainable solid adsorbent support for amine species in CO_2 adsorbents.

1.7. References

(1) Hansen, J.; Sato, M.; Kharecha, P.; Beerling, D.; Berner, R.; Masson-Delmotte, V.; Pagani, M.; Raymo, M.; Royer, D. L.; Zachos, J. C. Target Atmospheric CO2: Where Should Humanity Aim? *Open Atmos. Sci. J.* **2008**, *2*, 217–231.

(2) Karl, T. R.; Melillo, J. M.; Peterson, T. C. *Global Climate Change Impacts in the United States*; 2009; Vol. 54.

(3) U.S. Environmental Protection Agency. *Inventory of U.S. Greenhouse Gas Emissions and Sinks: 1990 - 2013*; 2015.

(4) Choi, S.; Drese, J. H.; Jones, C. W. Adsorbent Materials for Carbon Dioxide Capture from Large Anthropogenic Point Sources. *ChemSusChem* **2009**, *2* (9), 796–854.

(5) Serna-Guerrero, R.; Da'na, E.; Sayari, A. New Insights into the Interactions of CO2 with Amine-Functionalized Silica. *Ind. Eng. Chem. Res.* **2008**, *47* (23), 9406–9412.

(6) Bollini, P.; Didas, S. A.; Jones, C. W. Amine-Oxide Hybrid Materials for Acid Gas Separations. *J. Mater. Chem.* **2011**, *21* (39), 15100–15120.

(7) Goeppert, A.; Czaun, M.; Surya Prakash, G. K.; Olah, G. A. Air as the Renewable Carbon Source of the Future: An Overview of CO2 Capture from the Atmosphere. *Energy Environ. Sci.* **2012**, *5* (7), 7833–7853.

(8) Wei, J.; Liao, L.; Xiao, Y.; Zhang, P.; Shi, Y. Capture of Carbon Dioxide by Amine-Impregnated as-Synthesized MCM-41. *J. Environ. Sci.* **2010**, *22* (10), 1558–1563.

(9) Yue, M. B.; Chun, Y.; Cao, Y.; Dong, X.; Zhu, J. H. CO2 Capture by as-Prepared SBA-15 with an Occluded Organic Template. *Adv. Funct. Mater.* **2006**, *16* (13), 1717–1722.

(10) Xu, X.; Song, C.; Andresen, J. M.; Miller, B. G.; Scaroni, A. W. Novel Polyethylenimine-Modified Mesoporous Molecular Sieve of MCM-41 Type as High-Capacity Adsorbent for CO2 Capture. *Energy and Fuels* **2002**, *16* (6), 1463–1469.

(11) Leal, O.; Bolivar, C.; Sepulveda, G.; Molleja, G.; Martinez, G.; Esparragoza, L. Carbon Dioxide Adsorbent and Method for Producing the Adsorbent. U.S. Patent 5,087,597A, 1992.

(12) Zheng, F.; Tran, D. N.; Busche, B. J.; Fryxell, G. E.; Addleman, R. S.; Zemanian, T. S.; Aardahl, C. L. Ethylenediamine-Modified SBA-15 as Regenerable CO2 Sorbent. *Ind. Eng. Chem. Res.* **2005**, *44* (9), 3099–3105.

(13) Harlick, P. J. E.; Sayari, A. Applications of Pore-Expanded Mesoporous Silicas. 3. Triamine Silane Grafting for Enhanced CO2 Adsorption. *Ind. Eng. Chem. Res.* **2006**, *45* (9), 3248–3255.

(14) Huh, S.; Wiench, J. W.; Yoo, J.-C.; Pruski, M.; Lin, V. S.-Y. Organic Functionalization and Morphology Control of Mesoporous Silicas via a Co-Condensation Synthesis Method. *Chem. Mater.* **2003**, *15* (22), 4247–4256.

(15) Hicks, J. C.; Drese, J. H.; Fauth, D. J.; Gray, M. L.; Qi, G.; Jones, C. W. Designing Adsorbents for CO2 Capture from Flue Gas-Hyperbranched Aminosilicas Capable of Capturing CO2 Reversibly. *J. Am. Chem. Soc.* **2008**, *130* (10), 2902–2903.

(16) Liang, Z.; Fadhel, B.; Schneider, C. J.; Chaffee, A. L. Stepwise Growth of Melamine-Based Dendrimers into Mesopores and Their CO2 Adsorption Properties. *Microporous Mesoporous Mater.* **2008**, *111* (1-3), 536–543.

(17) Chaikittisilp, W.; Lunn, J. D.; Shantz, D. F.; Jones, C. W. Poly(L-Lysine) Brush-Mesoporous Silica Hybrid Material as a Biomolecule-Based Adsorbent for CO 2 Capture from Simulated Flue Gas and Air. *Chem. Eur. J.* **2011**, *17* (38), 10556–10561.

(18) Lavoine, N.; Desloges, I.; Dufresne, A.; Bras, J. Microfibrillated Cellulose – Its Barrier Properties and Applications in Cellulosic Materials: A Review. *Carbohydr. Polym.* **2012**, *90* (2), 735–764.

(19) Turbak, A. F.; Snyder, F. W.; Sandberg, K. R. Microfibrillated Cellulose. US4374702 A, 1983.

(20) Chanzy, H.; Dinand, E.; Maureaux, A.; Vignon, M. R.; Vincent, I. Microfibrillated Cellulose and Process for Making the Same from Vegetable Pulps Having Primary Walls, Especially from Sugar Beet Pulp. EP0726356 B1, 2002.

(21) Iwamoto, S.; Nakagaito, A. N.; Yano, H.; Nogi, M. Optically Transparent Composites Reinforced with Plant Fiber-Based Nanofibers. *Appl. Phys. A* **2005**, *81* (6), 1109–1112.

(22) Leitner, J.; Hinterstoisser, B.; Wastyn, M.; Keckes, J.; Gindl, W. Sugar Beet Cellulose Nanofibril-Reinforced Composites. *Cellulose* **2007**, *14* (5), 419–425.

(23) Plackett, D.; Anturi, H.; Hedenqvist, M.; Ankerfors, M.; Gällstedt, M.; Lindström, T.; Siró, I. Physical Properties and Morphology of Films Prepared from Microfibrillated Cellulose and Microfibrillated Cellulose in Combination with Amylopectin. *J. Appl. Polym. Sci.* **2010**, *117* (6), 3601–3609.

(24) Eriksen, Ø, Syverud, K. and Gregersen, Ø. The Use of Microfibrillated Cellulose Produced from Kraft Pulp as Strength Enhancer in TMP Paper. *Nord. Pulp Pap. Res. J* **2008**, *23* (3), 299–304.

(25) Engström, A.-C.; Ek, M.; Henriksson, G. Improved Accessibility and Reactivity of Dissolving Pulp for the Viscose Process: Pretreatment with Monocomponent Endoglucanase. *Biomacromolecules* **2006**, *7* (6), 2027–2031.

(26) Henriksson, M.; Henriksson, G.; Berglund, L. A.; Lindström, T. An Environmentally Friendly Method for Enzyme-Assisted Preparation of Microfibrillated Cellulose (MFC) Nanofibers. *Eur. Polym. J.* **2007**, *43* (8), 3434–3441.

(27) Aulin, C.; Gällstedt, M.; Lindström, T. Oxygen and Oil Barrier Properties of Microfibrillated Cellulose Films and Coatings. *Cellulose* **2010**, *17* (3), 559–574.

(28) Klemm, D.; Kramer, F.; Moritz, S.; Lindström, T.; Ankerfors, M.; Gray, D.; Dorris, A. Nanocelluloses: A New Family of Nature-Based Materials. *Angew. Chemie Int. Ed.* **2011**, *50*

(24), 5438–5466.

(29) Ho, T. T. T.; Zimmermann, T.; Hauert, R.; Caseri, W. Preparation and Characterization of Cationic Nanofibrillated Cellulose from Etherification and High-Shear Disintegration Processes. *Cellulose* **2011**, *18* (6), 1391–1406.

(30) Lam, E.; Male, K. B.; Chong, J. H.; Leung, A. C. W.; Luong, J. H. T. Applications of Functionalized and Nanoparticle-Modified Nanocrystalline Cellulose. *Trends Biotechnol.* **2012**, *30* (5), 283–290.

(31) Danon, A.; Stair, P. C.; Weitz, E. FTIR Study of CO2 Adsorption on Amine-Grafted SBA-15: Elucidation of Adsorbed Species. *J. Phys. Chem. C* **2011**, *115* (23), 11540–11549.

(32) Bacsik, Z.; Atluri, R.; Garcia-Bennett, A. E.; Hedin, N. Temperature-Induced Uptake of CO2 and Formation of Carbamates in Mesocaged Silica Modified with N-Propylamines. *Langmuir* **2010**, *26* (12), 10013–10024.

(33) Wang, X.; Schwartz, V.; Clark, J. C.; Ma, X.; Overbury, S. H.; Xu, X.; Song, C. Infrared Study of CO2 Sorption over "Molecular Basket" Sorbent Consisting of Polyethylenimine-Modified Mesoporous Molecular Sieve. *J. Phys. Chem. C* **2009**, *113* (17), 7260–7268.

(34) Hiyoshi, N.; Yogo, K.; Yashima, T. Adsorption Characteristics of Carbon Dioxide on Organically Functionalized SBA-15. *Microporous Mesoporous Mater.* **2005**, *84* (1–3), 357–365.

(35) Caplow, M. Carbamate Formation and Breakdown - Kinetics and Mechanism. **1968**, No. 8, 6795–6803.

(36) Pinto, M. L.; Mafra, L.; Guil, J. M.; Pires, J.; Rocha, J. Adsorption and Activation of CO2 by Amine-Modified Nanoporous Materials Studied by Solid-State NMR and 13CO2 Adsorption. *Chem. Mater.* **2011**, *23* (6), 1387–1395.

(37) Aziz, B.; Hedin, N.; Bacsik, Z. Quantification of Chemisorption and Physisorption of Carbon Dioxide on Porous Silica Modified by Propylamines: Effect of Amine Density. *Microporous Mesoporous Mater.* **2012**, *159*, 42–49.

(38) Bacsik, Z.; Ahlsten, N.; Ziadi, A.; Zhao, G.; Garcia-Bennett, A. E.; Martín-Matute, B.; Hedin, N. Mechanisms and Kinetics for Sorption of CO2 on Bicontinuous Mesoporous Silica Modified with N-Propylamine. *Langmuir* **2011**, *27* (17), 11118–11128.

CHAPTER 2

PROBING INTRAMOLECULAR VS. INTERMOLECULAR CO_2 ADSORPTION ON AMINE-GRAFTED SBA15

2.1. Background

Since most of the amine adsorbents studied for CO_2 capture have high amine loadings on the various supports, it may be presumed that CO_2 adsorption may often occur via cooperative interactions of two amines in different molecules or chains. However, a fundamental molecular level understanding of CO_2 adsorption requires insight into the propensity or probability for intramolecular vs. intermolecular cooperative adsorption when using amine molecules that contain multiple amine species. Very limited research to date has targeted intramolecular amine-amine interactions during CO_2 capture. Intramolecular interactions of amine sites in 3-(2-aminoethylamino)propyltrimethoxysilane (DI) molecules with CO_2 was suggested by Dibenedetto et al. based on CO_2 absorption studies under solution conditions.[1] They suggested that 3-(2-aminoethylamino)propyltrimethoxysilane species adsorbed CO_2 via intramolecular interactions using data from both ^{13}C and ^{1}H NMR spectra. However, these intramolecular interactions were observed in THF solvent, and if the mobility of the amine species is restricted via grafting to a solid surface, it is not clear if the same intramolecular interactions will occur, or if CO_2 adsorption would more favorably occur between two amines on adjacent molecules. Zheng et al.[2] grafted 3-(2-aminoethylamino)propyltrimethoxysilane (DI) on SBA15 and observed a larger amount of CO_2 was adsorbed on the sorbent functionalized with DI compared to reported literature related to 3-aminopropyltrimethoxysilane (MONO) adsorbent, which was interpreted as improvement of

performance due to intramolecular interactions of amines in DI. However, the carbamate species observed with FTIR can be formed due to either intramolecular or intermolecular interactions. Furthermore, since only one silane loading was tested for CO_2 adsorption, it was ambiguous if the increased CO_2 uptake for the DI adsorbent was a result of intramolecular interactions. Considering the chain length of the DI molecules, ~8.9 Å, the density of the silane groups (2.3 silane/nm^2 or 2.67 mmol silane/g) on the surface was sufficiently dense that CO_2 molecules could be adsorbed by intermolecular interactions as well. In other work, Knowles et al.[3,4] compared the adsorption of CO_2 on two different organosilane-grafted silica adsorbents. Specifically, solids modified with DI (0.8 silane/nm^2 or 1.60 mmol silane/g) and TRI aminosilanes (3-[2-(2-aminoethylamino)ethylamino]propyltrimethoxysilane) (0.75 silane/nm^2 or 1.52 mmol silane/g) were evaluated, and since the amount of CO_2 adsorbed on the two sorbents was similar, the adsorbed CO_2 was suggested to be adsorbed by intramolecular interactions. However, none of these studies explored CO_2 adsorption with a common, ultra-dilute surface coverage of the silanes, conditions that would make elucidation of intramolecular vs. intermolecular adsorption more facile. Additionally, the possibility of cooperative CO_2 adsorption by an amine and a surface silanol, as proposed by Bacsik et al., [5] also needs further exploration.

Measuring the isosteric heat of adsorption is a useful technique for probing adsorption heterogeneity.[6] Both the CO_2 uptake and heat evolved can vary with the types of amine sites, the nature of the amine-CO_2 bonding, the amine densities and the CO_2 partial pressure, and this behavior can give important insights into the nature of the surface interactions as well as the homogeneity or heterogeneity of the adsorption.[7] However, instead of measuring this value directly, the isosteric heat of adsorption has been most often calculated from adsorption isotherms (e.g. Langmuir,[8] Dubinin-astakhov,[9] Toth[10] isotherms) by application of the Clausius-Clapeyron

equation. Since this equation is based on the assumption of ideal gas behavior, applying it at elevated pressures may not be accurate. Nonetheless, numerous isosteric heat of adsorption values[11–14] have been calculated using the Clausius-Clapeyron equation, yet these values have not routinely been compared with experimental data measured by calorimetry. Several studies[15–18] have reported heats of adsorption of CO_2 with organosilane-modified adsorbents that were directly measured via calorimetry over various CO_2 pressure ranges. However, only one report[19] has described measured heats of adsorption at low CO_2 pressures relevant to low surface coverages (below 0.1 bar). Moreover, studies of isosteric heats of adsorption of CO_2 adsorption associated with intramolecular amine interactions have not been reported.

In this chapter, ultra-low loadings of four different organosilane molecules were grafted onto a mesoporous silica SBA15 support so that CO_2 could be adsorbed by primarily or only intramolecular amine interactions. The four grafted molecules studied contain four different functional moieties [propyl-amine, $SiCH_2CH_2CH_2NH_2$, (MONO); propyl-ethylenediamine, $SiCH_2CH_2CH_2NHCH_2CH_2NH_2$, (DI); propyl-diethylenetriamine, $SiCH_2CH_2CH_2NHCH_2CH_2NHCH_2CH_2NH_2$, (TRI); propyl-triethylenetetramine, $SiCH_2CH_2CH_2NHCH_2CH_2N(CH_2CH_2NH_2)_2$, (TREN)] including organosilanes that can only bind to form alkylammonium carbamates intermolecularly (MONO) as well as amines that can bind with inter- or intramolecular interactions (DI, TRI, TREN) to form alkylammonium carbamates. For a series of these samples, hexamethyldisilazane (HMDS) was used to cap accessible surface silanols and exclude the potential for CO_2 capture by amine interactions with silanols on the surface, which is hypothesized to give carbamic acid species.[20] The CO_2 uptake over various CO_2 partial pressures was measured over these adsorbents, and simultaneously, the isosteric heats of adsorption of CO_2 were measured. The potential for intramolecular CO_2 adsorption has been

explored and the effective distances between two amine molecules for CO_2 adsorption via intramolecular interactions was estimated for each silane. The insights from this work may be utilized in the design of new amine molecules that might have improved sorption properties, while the collected data provide new understanding of the mechanism and kinetics of CO_2 adsorption at low amine loadings.

2.2. Experimental

Materials

All chemicals (higher than Reagent Grade purity) were used without further purification. Poly(ethylene glycol)-block-poly(propylene glycol)-block-poly(ethylene glycol) (Pluronic P123, M_n ~5800), tetraethylorthosilicate (TEOS), hexamethyldisilazane (HMDS), anhydrous toluene, di-*tert*-butyl dicarbonate, sodium carbonate (Na_2CO_3), sodium hydroxide (NaOH), magnesium sulfate ($MgSO_4$), dichloromethane and triethylamine were purchased from Sigma-Aldrich. Hydrochloric acid (HCl, 37%), methanol, hexane, ethyl acetate and chloroform were purchased from EMD. Tris(2-aminoethyl)amine (TREN) was purchased from Alfa Aesar. 3-aminopropyl trimethoxysilane (MONO), 3-(2-Aminoethylamino)propyltrimethoxysilane (DI), 3-[2-(2-aminoethylamino)ethylamino]propyltrimethoxysilane (TRI) and 3-iodopropyltrimethoxysilane were purchased from Gelest.

Preparation of SBA15

SBA15 was synthesized as reported in the literature.[21] In brief, 24 g of Pluronic P123 copolymer was dissolved in 120 mL of HCl and 636 g of DI water in a 2000 mL Erlenmeyer flask. The solution was stirred at 40 ºC until the polymer was fully dissolved. To this solution, 46.26 g

of TEOS was slowly added and stirred at 40 ºC for 20 h. Then, the mixture was heated to 100 ºC for 24 h without stirring. The reaction mixture was quenched with 400 mL of DI water and white precipitant was filtered and washed with copious DI water. The white precipitant was dried overnight at 75 ºC and dried material was calcined with following procedure: i) ramp to 200 ºC at 1.2 °C/min, ii) hold at 200 ºC for 1 h, iii) ramp to 550 ºC at 1.2 ºC/min, iv) hold at 550 ºC for 12 h, v) cool to room temperature at 10 ºC/min.

Grafting of MONO, DI, and TRI silanes onto SBA15

First, 1 g of fully dried SBA15 was dispersed in 75 mL of anhydrous toluene. MONO, DI or TRI silane was the added to the mixture and stirred at room temperature for 24 h under a nitrogen atmosphere. For the preliminary studies of isolated grafting condition, various amount of MONO, DI or TRI silanes (0.2–2.2 mmol silane/g) were added. The product was filtered and washed several times with toluene, hexane and methanol. The residue was dried under vacuum overnight at 60 °C.

Synthesis of boc protected TREN (2P-TREN)

Two primary amines of TREN were protected by following a literature procedure.[22] First, 100 mmol of TREN was dissolved in 50 mL of anhydrous dichloromethane and cooled to 0 °C. Then, 100 mmol of di-*tert*-butyl dicarbonate dissolved in 50 mL of anhydrous dichloromethane was added dropwise to the TREN mixture and stirred at room temperature for 24 h. The solvent was removed under vacuum and the remaining oil was dissolved in ethyl acetate and washed with 0.5 M of NaOH. The remaining water in the organic phase was removed by $MgSO_4$ and the purified organic phase was recovered via filtration. The solvent was removed by rotary evaporation. The yellow oil was dissolved in a mixture of dichloromethane and methanol (90/10,

v/v). The final product was purified by using silica chromatography. The fractions containing the desired product were verified with TLC and ^{1}H NMR, which is shown in Figure 2.1.

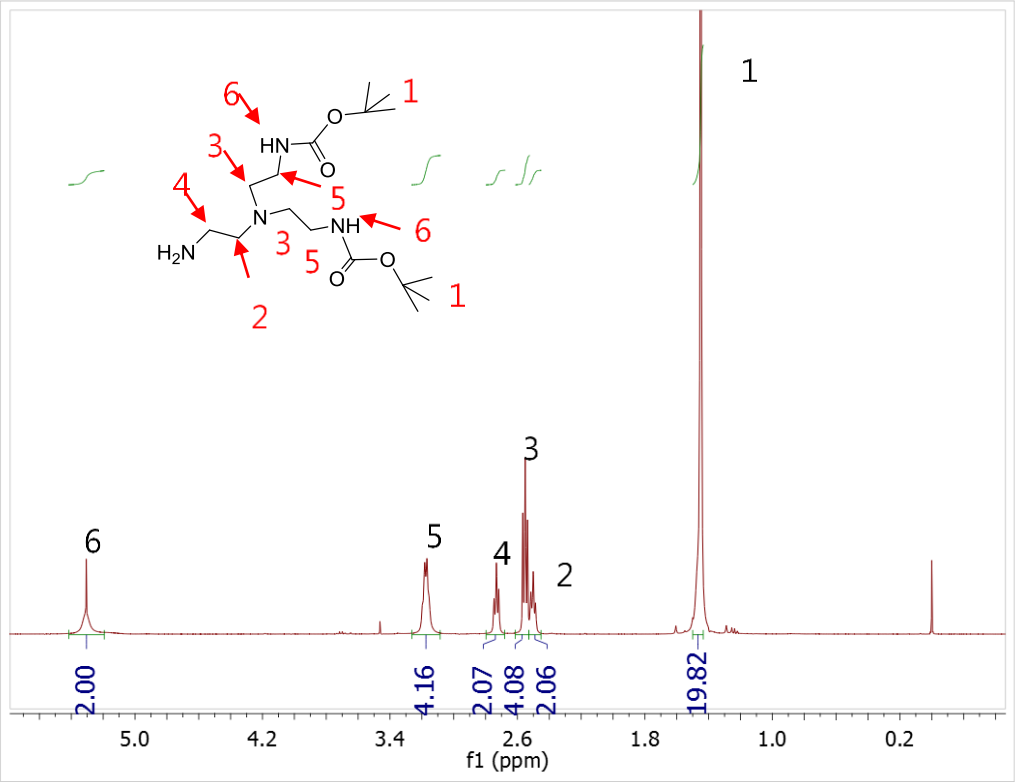

Figure 2.1. ^{1}H NMR spectrum of 2P-TREN. ^{1}H-NMR (400 MHz, $CDCl_3$, δ): 1.37 (s, 18 H), 2.38-2.44 (m, 6 H), 2.49-2.54 (m, 2 H), 2.95 (m, 4 H), 5.30 (s, 2 H).

Synthesis of TREN modified SBA15

First, 1 g of SBA15 was dispersed in 75 mL of anhydrous toluene. Next, 12.5 mmol of 3-iodopropyltriemthoxysilane was added at room temperature and stirred at 100 °C for 24 h. The iodopropyl grafted SBA15 (I-SBA15) was filtered and washed with copious toluene, hexane and methanol. The residue was dried under vacuum overnight at 60 °C. To substitute the iodine species of I-SBA15 with TREN molecules, 1 g of I-SBA15 was dispersed in 30 mL of anhydrous toluene. Then, 0.8 mmol of 2P-TREN and 1.2 mmol of triethylamine were added to the slurry mixture and

refluxed for 12 h. The solution was filtered and washed with toluene, hexane, methanol, ammonium hydroxide. After drying the white powder, the 2P-TREN modified SBA15 was re-dispersed in a mixture of methanol and hydrochloride solution (100/1, v/v) to deprotect the *tert*-butyloxycarbonyl (boc) protecting groups. The mixture was stirred at 60 °C for 6 h and then washed with methanol. To neutralize the protonated amines, the product was dispersed in Na_2CO_3 saturated methanolic solution. The product was then filtered and washed with methanol and dried under vacuum overnight at 60 ºC, to yield the TREN adsorbent material.

Capping silanols on amine-grafted SBA15

After grafting organosilane molecules on SBA15, the exposed silanols on the surface of adsorbents were capped by HMDS. In brief, 1 g of amine functionalized SBA15 was dispersed in 40 mL of HMDS and stirred at room temperature for 24 h. Then remaining powder was filtered and washed several times with chloroform. The final product was dried under vacuum overnight at 60 °C.

Physical Characterization

The specific surface areas and pore volumes of the adsorbents were calculated or measured from nitrogen physisorption isotherms obtained at 77 K (Tristar II 3020, Micrometrics). Before each analysis, the samples were degassed under 30 mTorr of vacuum at 120 °C for 12 h. The specific surface areas of the adsorbents were calculated by the BET method and pore size distributions of the adsorbents were analyzed by the NLDFT equilibrium kernal for N_2 adsorption onto silica via the Quantachrome VersaWin software package. Elemental compositions of the adsorbents were measured at Atlantic Microlab (Norcross, GA). C and N analyses were performed

by combustion using an automatic analyzer. Iodine analysis was performed by flask combustion followed by ion chromatography. All samples were dried at 100 °C under vacuum prior to the measurements. The chemical structures of the synthesized molecules were verified by NMR (solution state ^{1}H NMR, Bruker DMX 400 and solid state ^{13}C NMR, Bruker DSX 400).

CO_2 adsorption and isosteric heat measurements

CO_2 adsorption capacities for the array of amine-grafted SBA15 materials were measured by TGA (Q500, TA instruments) analysis. Each sample was pretreated under He flow at 110 °C for 3 h and subsequently equilibrated at 30 °C. Then, the samples were exposed to 90 ml/min of 400 ppm CO_2/He gas for 12 h. CO_2 adsorption capacities and heats of adsorption for the array of low loading (<0.45mmol silane/g) amine-grafted SBA15 materials were measured by a combined calorimeter-volumetric adsorption apparatus, which consists of a gas dosing manifold and a Tian-Calvet Calorimeter (Sensys Evo DSC, Setaram).[19,23] The powder sample was first pressed at 1000 psi[24] and then crushed into pellets (150-250 μm). Subsequently, 50 mg of the pellets were inserted in one side of sample cell that has two prongs. Another side of the cell was left empty as a reference. This cell is connected to the dosing manifold and encased in an aluminum block that contains highly sensitive thermophiles. The samples were pretreated at 120 °C for 3 h under 15 Pa of vacuum and then the temperature was cooled down to 30 °C. Two pressure transducers were connected to the reservoir and cell areas, which were maintained at 30 °C with heating tape. The amount of adsorbed CO_2 after dosing was calculated by mole balance using initial and final pressure values from the cell and reservoir sides. Heats of CO_2 adsorption were simultaneously recorded while the dosed CO_2 was adsorbed by the adsorbents. When the rate of pressure change

became lower than 10^{-2} Pa/min, the system was considered to have reached a pseudo-equilibrium state.

2.3. Results and discussions

Synthesis of SBA15

The nitrogen adsorption–desorption isotherm profiles and pore size distribution of the calcined, bare SBA15 support are presented in Figure 2.2. The hysteresis loop showed the conventional mesoporous structure of SBA15, with a narrow pore size distribution (8 nm). The synthesized SBA15 showed a similar surface area (799 m^2/g) and pore volume (0.95 cm^3/g) compared to the literature data.[21]

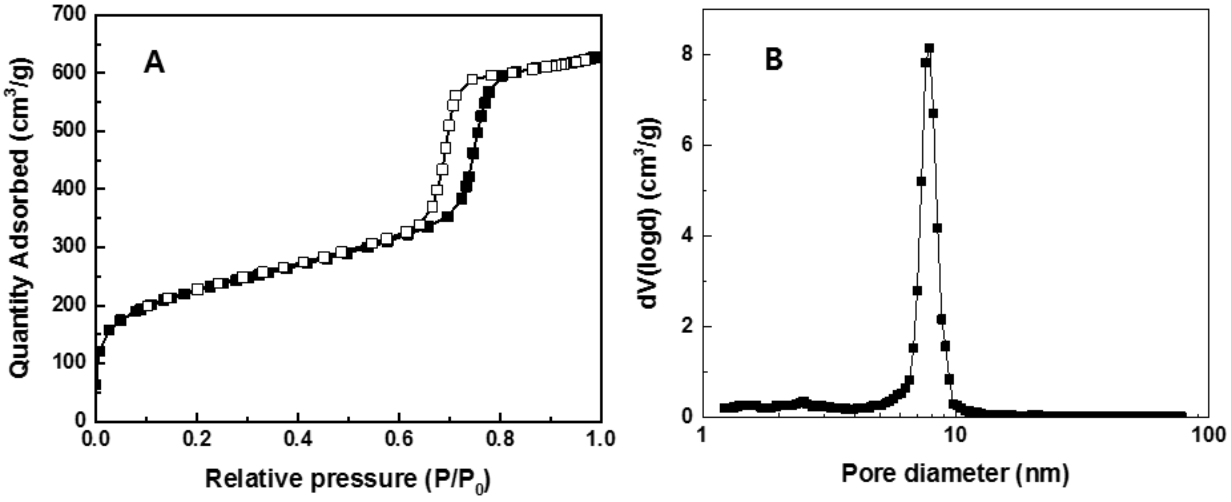

Figure 2.2. (A) Nitrogen adsorption-desorption isotherms of unfunctionalized SBA15 and (B) pore size distribution of unfunctionalized SBA15

Organosilane species on the SBA15

The molecular structure and nomenclature of amine adsorbents are shown in Figure 2.3. All the organosilanes contain a propyl chain as the surface linking group to the first amine, with silanes having additional amines having separations of two methylene units between each amine. According to the structure of amine molecules attached at the propyl chain, the adsorbents were named MONO, DI, TRI and TREN (Figure 2.3). In the case of silanol capped adsorbents, the prefix, HMDS, was added to the sample name. (e.g. HMDS-MONO)

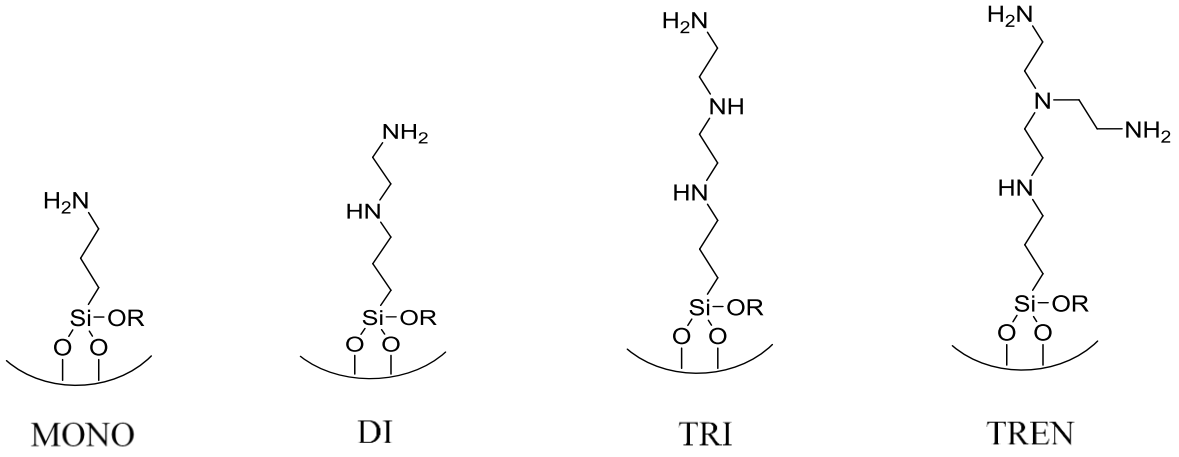

Figure 2.3. Molecular structure of grafted onto SBA15. Note surface linkage likely include those with one, two and three siloxane bonds to the oxide surface.

Isolated grafting condition for intramolecular interaction

By measuring the CO_2 uptake along with different organosilane molecules grafted on same support material at various loadings, the amount of grafted silane molecules that equate to isolated conditions can be indirectly inferred. Figure 2.4 shows the CO_2 adsorption capacities of adsorbents based on the silanes described above with various loadings (0.2-2.2 mmol silane/g) of organosilane molecules. The CO_2 uptake increased as the silane loading density increased, as expected for

alkylammonium carbamate formation. It can be noted that there is a specific organosilane loading in each case where the CO_2 uptake began to steeply increase. The threshold organosilane loading varied according to the nature of the silane molecules grafted onto the support. For the MONO sorbent, this threshold loading was between 0.9-1.4 mmol silane/g. Owing to the presence of only one amine on each MONO molecule, this family of materials had the lowest uptake at low organosilane loadings, likely associated with amine-silanol interactions and/or a very small amount of paired organosilane sites on the silica surface, yielding alkyl ammonium carbamates. In contrast, the CO_2 uptakes for the DI and TRI adsorbents were higher at low organosilane loadings, significantly exceeding the CO_2 uptakes of the MONO sample by an organosilane loading of 0.4-0.6 mmol/g. It can further be observed that the point at which each curve has a steep upturn occurs in the order TRI>DI>MONO, consistent with the longer chain silanes having a propensity to form intermolecular pairs at a lower silane loading.

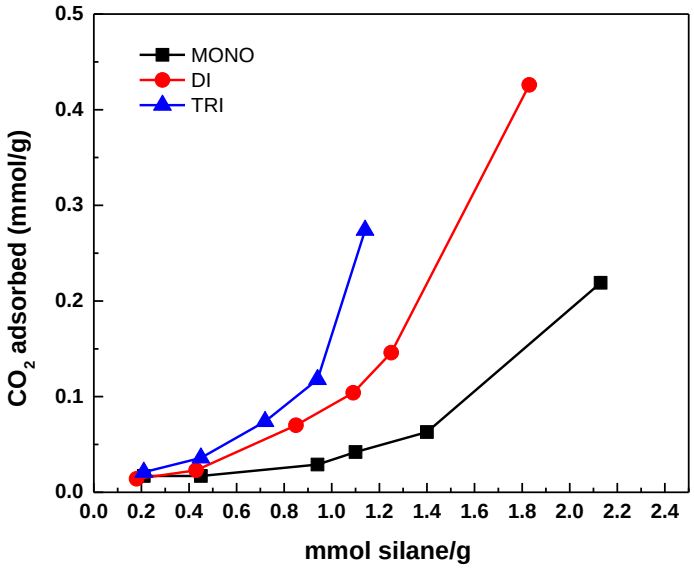

Figure 2.4. CO_2 uptake as a function of silane loading for MONO, DI or TRI silane species grafted onto SBA15.

From the collected data, one may infer that adsorption at the smallest loadings was primarily from intramolecular adsorption for materials based on the DI and TRI silanes, and it may inferred that CO_2 molecules were captured by a combination of intermolecular as well as intramolecular interactions at the higher loadings, with the steep rise associated with the onset of significant intermolecular interactions. Thus, adsorbents with a silane loading less than 0.45 mmol silane/g were chosen to elucidate the propensity for intramolecular interactions yielding CO_2 adsorption.

Structure properties of organosilane grafted (<0.45 mmol silane/g) adsorbents

The specific surface areas and pore volumes of the organosilane-grafted samples are listed in Table 2.1. After grafting organosilane molecules onto the SBA15 support, similar specific surface areas (415-450 m^2/g) and pore volumes (0.63-0.70 cm^3/g) were observed for all the adsorbents. In the case of HMDS modified adsorbents, since the silanol groups on the surface were additionally capped by HMDS, lower surface areas (328-350 m^2/g) and pore volumes (0.54 cm^3/g) were obtained in comparison with the uncapped adsorbents.

The total amine loading and carbon to nitrogen weight ratio of the adsorbents are also summarized in Table 2.1. The loading of silane molecules on the MONO, DI, TRI and TREN adsorbents was calculated by dividing the total amine loading by 1, 2, 3 and 4, respectively. The theoretical C to N weight ratio for each adsorbent was calculated based on the following assumptions, as given in the Table 1: (i) only one alkoxy group of a silane molecule was hydrolyzed (ii) two alkoxy groups of a silane molecule were hydrolyzed, or (iii).three alkoxy groups of a silane molecule were hydrolyzed. The experimentally observed C to N weight ratios

of all the uncapped adsorbents were consistent with about two siloxane bonds to the surface (MONO, DI) or approximately one to two siloxane bonds to the surface (TRI, TREN).

Table 2.1. Organic molecule loading amount, weight ratio of C/N, specific areas and pore volumes of adsorbents.

Samples	Specific surface area (m^2/g)	Pore volume (cm^3/g)	Amine groups (silane molecules) [a] mmol/g	C/N weight ratio (theoretical ratio i/ii/iii)[b]
Bare SBA15	799	0.95	n/a	n/a
Mono	450	0.70	0.45(0.45)	3.42 (4.28/3.43/2.57)
Di	415	0.68	0.85(0.42)	2.63 (3.00/2.57/2.14)
Tri	422	0.63	1.29(0.43)	2.45 (2.57/2.29/2.00)
TREN	420	0.67	0.82(0.29)	2.25 (2.36/2.14/1.93)
HMDS-SBA15	442	0.68	n/a	n/a
HMDS-MONO	328	0.54	0.41(0.41)	n/a
HMDS-DI	332	0.54	0.82(0.41)	n/a
HMDS-TRI	350	0.54	1.05(0.35)	n/a

[a]Silane loadings were calculated by dividing the total amine loading with the number of amines in the specific organosilane molecule.; [b](i) Only one alkoxy group of a silane molecule was hydrolyzed (ii) two alkoxy groups of a silane molecule were hydrolyzed, or (iii).three alkoxy groups of a silane molecule were hydrolyzed.

In the case of the TREN adsorbent, trace iodine was not detected by elemental analysis, which suggested that all of the iodo species of the precursor, 3-iodopropyltrimethoxysilane, were substituted by primary amines of 2P-TREN. The successful removal of *tert*-butyloxycarbonyl (boc) protecting groups from the primary amines of TREN was verified by solid state ^{13}C NMR

(Figure 2.5). The carbonyl peak of the tert-butyloxycarbonyl protecting group was not observed at 160 ppm after deprotection. Considering that C to N weight ratio and the observed chemical shifts in the solid state 13C NMR spectra for the TREN adsorbent, it can be inferred that the desired propyl-triethylenetetramine structure was synthesized, as shown in Figure 2.3.

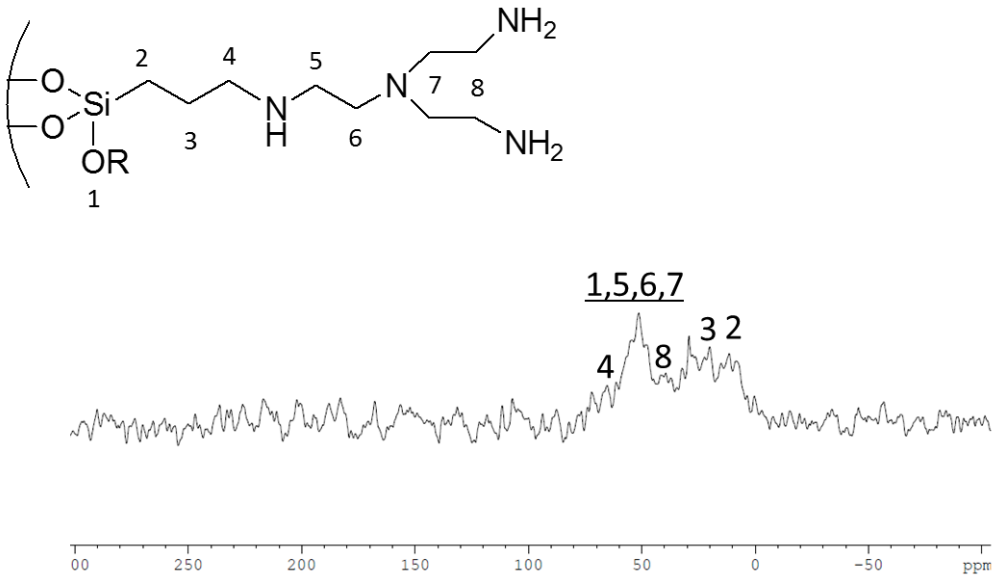

Figure 2.5. Solid state (CP-MAS) ^{13}C NMR spectrum of TREN adsorbent.

Average distances between adjacent silane molecules

With these low loading adsorbents, the average distances between two adjacent silane molecules on the surface were estimated and listed in Table 2.2. As a first step of approximation for the distances, the average density of organosilanes on each adsorbent was calculated by dividing the number of silane molecules with the surface area (799 m^2/g) of the bare SBA15. Then, the maximum silane molecule domain area was calculated as the inverse of the density of silane molecules. These domains were assumed to be circular in shape, and based on this assumption, the average radius of the silane domains for each case were calculated (Table 2.2).

Table 2.2. The length of alkyl chain, grafting density, silane domain areas for low loading (<0.45 mmol silane/g) silane adsorbents and average distances between adjacent silane molecules on the surface.

Samples	[a] Length of organosilane chain (Å)	[b] Density of silane molecules, D (number/nm^2)	Average silane domain area, 1/D (nm^2)	[c] Average radius of silane domain, R (Å)
MONO	5.2	0.34 (0.42)[d]	2.95 (2.36)	9.7 (8.7)
DI	8.9	0.32 (0.40)	3.16 (2.53)	10.0 (9.0)
TRI	12.4	0.32 (0.40)	3.09 (2.47)	9.9 (8.9)
TREN	12.4	0.22 (0.27)	4.58 (3.67)	12.1 (10.8)

[a]Length of the organosilane (between terminal primary amine and Si atom) molecule was estimated using Chemdraw 3D Ultra software.; [b]Average density of silane molecules, D, was calculated by dividing the number of silane molecules with the surface area (799 m^2/g) of bare SBA15.; [c]Average radius of silane domain, R, was calculated with the following equation. $R = \sqrt{\frac{1}{D \times \pi}}$ This equation is based on the assumption that each silane molecule occupies a circular area of the surface shape area.; [d]The values in parenthesis represent calculated values based on the combined mesopore (pores >1.24 nm) + external surface area, 640 m^2/g in total.

The values in parenthesis represent calculated value based on the combination of the mesopore surface area and the external surface area (640 m^2/g). In the literature, the average silane density has been usually calculated based on the total surface area of the bare support. However, it is unlikely that micropores play a role in silane grafting, and the highly reduced micropore surface area after grafting of the organosilanes on the support was observed from all samples (Table 2.3), suggesting that added organosilanes block the very small micropores of the SBA15. Considering the length of the organosilanes (5.2-12.4 Å) and the steric hindrances in the micropores, the organosilanes are expected to easily block the micropore entrances. Comparing

the average radius of silane domain and the length of each organosilane between the terminal primary amine and Si atom, as estimated by Chemdraw 3D Ultra software, it was inferred that two adjacent silane molecules were typically grafted far enough apart so that CO_2 molecules would be primarily captured by intramolecular interactions at the targeted silane loading. Specifically, as noted in Table 2.2, on average, MONO and DI sorbents have the silanes sufficiently spaced such that intermolecular interactions are quite limited, meaning that CO_2 capture should occur exclusively by intramolecular sorption between two amines on a single silane (DI), between an amine and a silanol (MONO, DI), or via intermolecular interactions between two amines on different silanes (MONO, DI, with low probability due to average amine spacing). Even for the TRI and TREN silanes, the average spacing should be sufficient to favor intramolecular CO_2 sorption over interactions between adjacent silane molecules.

Table 2.3. Micropore surface area and mesopore+external surface areas for amine functionalized adsorbents.

Samples	Mircopore surface area (m^2/g)	Mesopore + external surface area (m^2/g)
Bare SBA-15	160	640
MONO	33	417
DI	0	415
TRI	0	422
TREN	15	405

CO_2 adsorption with amine adsorbents containing silanols

The CO_2 capacities and silane molecule efficiencies for the adsorbents as a function of CO_2 pressure are shown in Figure 2.6. Note that silane molecule efficiencies (mol CO_2 / mol silane) are being used here instead of the traditional amine efficiencies commonly discussed in the literature (mol CO_2 / mol N), because of the focus on potential intramolecular amine adsorption. Since bare SBA15 has no functional groups that can chemically adsorb CO_2, the primary mode of adsorption of CO_2 by SBA15 is physical adsorption at the surface silanols, and thus the amount of CO_2 adsorbed on SBA15 increased linearly with increasing CO_2 pressure. On the other hand, the other adsorbents showed a nonlinear increase of CO_2 uptake at low CO_2 pressure (below 3000 Pa) and the CO_2 uptake increased proportional to the dosed CO_2 pressure at high pressures (over 3000 Pa). It can be inferred that CO_2 molecules were mainly adsorbed by chemical adsorption at lower pressures and physical adsorption became important at high CO_2 pressures. Aziz et al.[25] estimated the relative amounts of chemisorption and physisorption of CO_2 molecules on MONO-modified mesoporous silica using the distinctly different FTIR peaks associated with physisorbed (2341 cm^{-1}) and chemisorbed (1490, 1571 cm^{-1}) CO_2. When the CO_2 pressure was 10.0 torr, most of CO_2 adsorption originated from chemisorption and the ratio of physisorption to chemisorption of CO_2 on the silica increased with CO_2 pressure. Based on the slope of the CO_2 isotherms in Figure 2.6, it is suggested that physisorption of CO_2 for MONO, DI, TRI and TREN adsorbents became important after loadings of 0.01, 0.035, 0.09 and 0.07 mmol CO_2/g, respectively. Under an assumption that the organosilanes were well dispersed and on average, isolated, on the adsorbents, the increased CO_2 uptake of the MONO, DI, TRI and TREN adsorbents, compared to bare SBA15, suggests that CO_2 might be captured by intramolecular interactions as more amines are added to each silane molecule

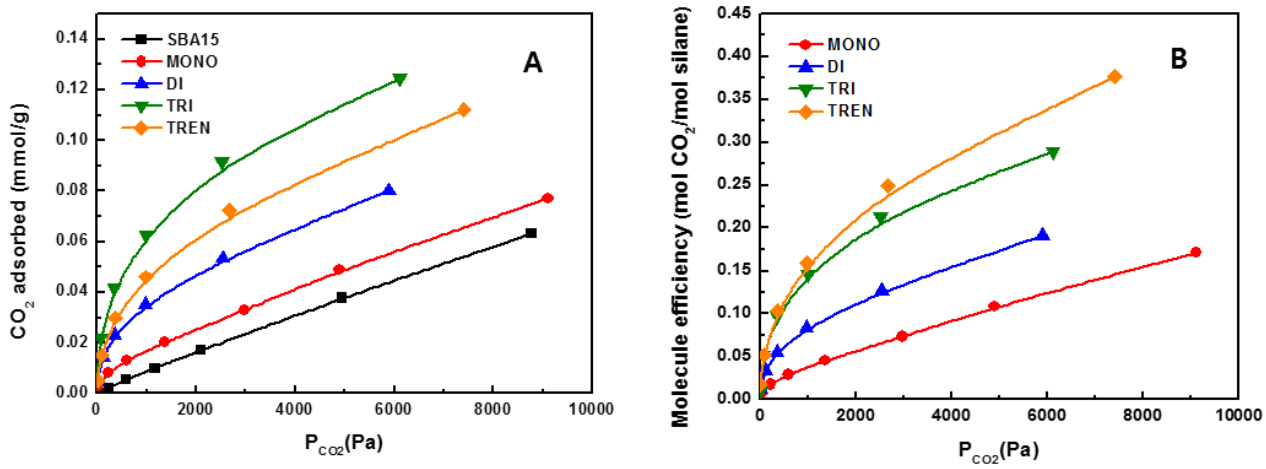

Figure 2.6. Adsorption isotherms expressed as CO_2 capacities (A) and silane molecule efficiencies (B) for the amine functionalized SBA15 materials.

In terms of silane molecule efficiency, the adsorbents that contained a larger number of amines in one silane molecule had an enhanced silane molecule efficiency (Figure 2.6 B). This means that the number of possible cooperative CO_2 capture pairs would be increased based on the number of amine moieties in a single silane molecule. However, a significant increase in silane molecule efficiency for the TREN adsorbent over the TRI adsorbent was not observed.

Cooperative amine pairs for CO_2 capture

The hypothesized intramolecular interaction pairs under the employed dry CO_2 adsorption conditions are summarized in Table 2.4. Danon et al.[20] reported that CO_2 may be adsorbed by amine-silanol interactions as well as by adjacent amine pairs. For these pairs, the organosilane molecules need to be flexible so that the amine molecules can interact with the surface silanols on the adsorbents. Even though the potential for CO_2 capture by two identical amines (eg. NH_2-NH_2, NH-NH, N-N interactions) under dry conditions has been explored,[26] CO_2 capture via the exclusive

interactions between two different amines (excluding the potential for intermolecular amine-amine interactions, as may occur with DI and TRI at high organosilane loadings) has rarely been studied. Work by Didas et al.[27] and Brunelli et al.[28] suggest that the length of the propyl chain of MONO is sufficient for the amines to interact with silanols on the surface of SBA15. Thus, under the ultra-dilute organosilane loading conditions, the MONO adsorbent has only one likely CO_2 capture pair, the primary amine (NH_2)-surface silanol (OH) pair. (Table 2.4)

The DI adsorbent has two more possible CO_2 capture pairs (Table 2.4), in addition to the NH_2-OH interaction. A secondary amine (NH) may pair with a primary amine (intramolecular cooperative amine adsorption) or with a silanol, to facilitate CO_2 capture.

Table 2.4. Hypothesized potential cooperative pairs for CO_2 capture under dry conditions with different isolated organosilane-modified adsorbents

Samples	Possible cooperative pairs for CO_2 capture under dry condition					
MONO	NH_2-OH					
DI	NH_2-OH	NH-OH	NH_2-NH			
TRI	NH_2-OH	NH-OH x2	NH_2-NH x2	NH-NH		
TREN	NH_2-OH x2	NH-OH	NH_2-NH_2	NH_2-NH x2	NH_2-N x2	NH-N

To date, knowledge about the distance between primary and secondary amines required for effective CO_2 adsorption via intramolecular interactions has not been directly explored. If the distance between two amines (NH_2, NH) of the DI adsorbent (i.e. -CH_2CH_2-) is suitable for capturing CO_2, then NH-NH and NH_2-NH interactions might also be useful for CO_2 capture using

the TRI material. In the case of NH_2-NH interactions for the TRI adsorbent, two different NH_2-NH interactions are possible as follows: (i) primary amine - secondary amine, with a two atom spacer (i.e. -CH_2CH_2-), (ii) primary amine - secondary amine, with a 5 atom spacer (i.e. -CH_2CH_2NH CH_2CH_2-).

The length of the linear linking chain for the TREN adsorbent is the same as for the TRI adsorbent (Table 2.2), but it has one more additional branch that contains another primary amine (Figure 2.3). This organosilane, which has been rarely studied,[29] contains two primary amines, one secondary amine, and one tertiary amine. Thus, CO_2 molecules can be adsorbed by primary - primary interactions, with a five atom linker (i.e. -$CH_2CH_2NCH_2CH_2$-). Primary–secondary interactions are also possible, with a five atom linker (i.e. -$CH_2CH_2NCH_2CH_2$-). Primary–tertiary interactions are possible, as well, with the primary amine binding the CO_2 and the tertiary accepting a proton, with a two atom linker (i.e. -CH_2CH_2-). Finally, amine–silanol cooperation is also possible for TREN. It is anticipated that secondary–tertiary amine cooperation would be disfavored due to steric constraints, so it is not considered here.

CO_2 adsorption with silanol capped adsorbents

To explore the potential for sorption via amine–silanol interactions owing to the flexibility of the alkyl chains of the organosilanes, the silanol groups of the adsorbents were capped by HMDS and the CO_2 uptakes of the materials were measured. The CO_2 capacities and silane molecule efficiencies for these HMDS-capped adsorbents are shown in Figure 2.7. Since the amine species in the HMDS-capped adsorbents cannot interact with silanols, it can be inferred that any CO_2 adsorption above the level of the bare, capped support likely originated by intramolecular interactions of two amines. For the HMDS-MONO material, CO_2 molecules cannot be chemically

adsorbed by two adjacent primary amines because the aminosilane molecules were effectively isolated at an organosilane loading of 0.45 mmol/g (Table 2.1).

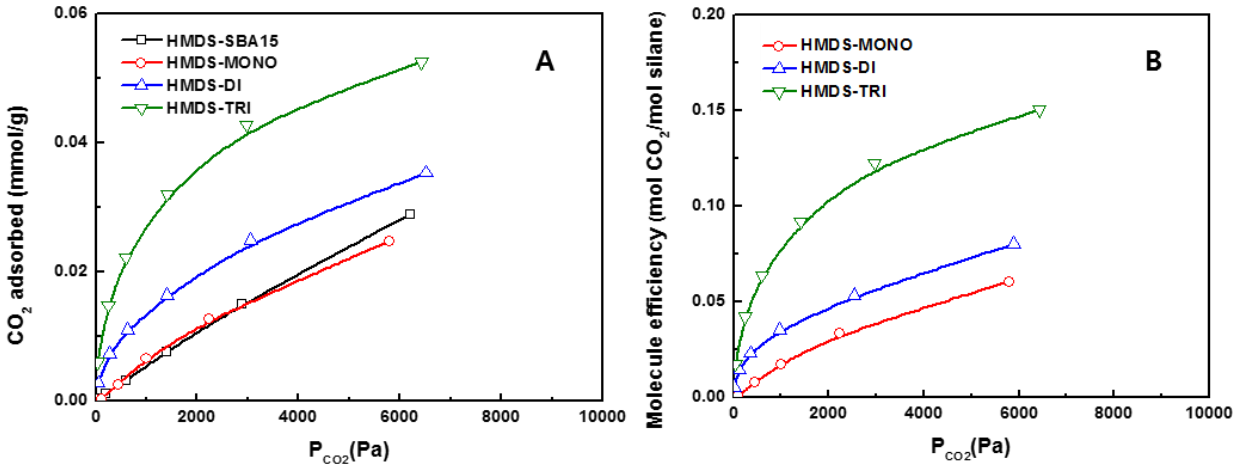

Figure 2.7. Adsorption isotherms expressed as CO_2 uptake (A) and silane molecule efficiency (B) for amine functionalized HMDS-capped adsorbents.

The isolation of the organosilanes on the MONO adsorbent was further verified by comparison of the CO_2 uptake of HMDS-MONO and HMDS-SBA15, which were similar (Figure 2.7). By removing the silanols, the isolated amines had no pairing partners, and the CO_2 uptake was reduced. In contrast, for both HMDS-DI and HMDS-TRI, the adsorption capacities were elevated above the capacity displayed by the capped, amine-free support. This observation strongly asserts that these two sorbents do adsorb CO_2 via intramolecular amine-amine interactions. While the CO_2 capacities for the HMDS-adsorbents were significantly reduced in comparison with the uncapped adsorbents, it cannot be firmly concluded that most of adsorbed CO_2 by the uncapped adsorbents resulted from amine interactions with silanols. Because of the reduced surface areas of the HMDS-adsorbents, the amount of physically adsorbed CO_2 also decreased compared to the bare SBA15 (Figure 2.6A, 2.7A), which affected the slope of the CO_2 adsorption in the high pressure range. On top of that, the higher hydrophobicity of the HMDS modified surfaces might

have an effect on the adsorption of CO_2 via alkylammonium carbamate formation. These charged species can undoubtedly be better accommodated on the polar surface environment created by surface silanols, being likely disfavored by creation of a hydrophobic trimethylsilyl covered surface.

Effective alkyl chain length between two amines for intramolecular interactions

As noted above, the CO_2 uptake of HMDS-MONO was similar to that of HMDS-SBA15 and proportional to the dosed CO_2 pressure, which indicated that the CO_2 molecules were likely physically adsorbed on this material, suggesting no productive amine-CO_2 binding in this case. Brunelli et al.[28] also reported reduced amine efficiency, from 0.22 to 0.10, after capping silanols of a 3-aminopropyltrimethoxysilane modified adsorbent, and the CO_2 capacity for the adsorbent was less than that of bare, silanol-containing SBA15. The HMDS-DI and HMDS–TRI adsorbents showed higher CO_2 uptakes than the HMDS-MONO adsorbent. While the HMDS-MONO adsorbent showed a silane molecule efficiency of 0.02 at 1000 Pa of CO_2 pressure, the HMDS-DI and HMDS–TRI adsorbents showed values of 0.04 and 0.08 (interpolated), respectively. This suggests that the amines in the HMDS-DI and HMDS-TRI adsorbents could capture CO_2 via intramolecular amine interactions. Interestingly, it is noteworthy that the difference of the silane molecule efficiency between HMDS-DI (0.07) and HMDS–TRI (0.14) adsorbents at 6000 Pa was much higher than that of HMDS-MONO (0.05) and HMDS–DI (0.07) adsorbent at the same partial CO_2 pressure. Even though the amines in the HMDS-DI adsorbent could likely adsorb CO_2 molecules via intramolecular interactions, as shown Figure 2.7, it does not appear to do so efficiently. This may be because the distance between the primary and secondary amine (i.e. NH-CH_2-CH_2-NH_2) appears not to be long enough to capture significant amounts of CO_2 under these

conditions. On the other hand, the HMDS-TRI sample showed a higher silane molecule efficiency than the HMDS-DI adsorbent. Since the distance between the primary amine and secondary amine close to the primary amine is the same as in the DI material (hypothesized above to not very effectively capture CO_2), the increased silane molecule efficiency of HMDS-TRI might be mainly caused by the interaction between the primary amine and the secondary amine close to the silicon atom (i.e. five atom linker, -CH_2CH_2NH CH_2CH_2-). Consequently, based on these results, the high CO_2 uptake of the TRI adsorbent may likely be attributed to the combination of amine interactions with silanols and other amines in the same alkyl chain, likely the primary and secondary amines separated by 5 atoms.

Hypothesized species resulting from the CO_2 chemisorption

Figure 2.8 shows an array of hypothesized chemisorbed CO_2 species on the organosilane modified SBA15 silica materials studied here. When CO_2 molecules are adsorbed by amine interactions with silanols for the MONO adsorbent, three primary species are likely formed (i) carbamic acid species interacting with a silanol group via a hydrogen bond, ii) bound carbamate species (silylpropylcarbamate), and (iii) alkylammonium carbamate species. Aziz et al.,[25] Danon et al.,[20] and Didas et al.[30] have previously assigned FTIR bands associated with adsorbed CO_2 to these species (Figure 2.8, top left). It may be expected that the silanol-CO_2-amine species may be formed when the density of organosilanes on the surface of adsorbent is low, leaving many free silanols. If the water is removed from this species (carbamic acid), the bound carbamate species would be able to form slowly on the surface, as postulated in an FTIR study of Bacsik et al.[5] Since CO_2 molecules cannot be chemisorbed by a single amine alone, under dry conditions, if the silanols of the MONO adsorbent are capped, CO_2 cannot be chemically adsorbed on this adsorbent (Figure

2.8, top right). According to the FTIR data of Danon et al.,[20] no chemisorbed CO_2 species were observed on capped isolated MONO adsorbent. This is consistent with our data shown in Figure 2.7. In the case of the DI, TRI and TREN adsorbents, carbamate species via intramolecular interaction of amines may form, as well as carbamic acid and silylpropylcarbamate species by amine interaction with silanols (Figure 2.8, bottom left).

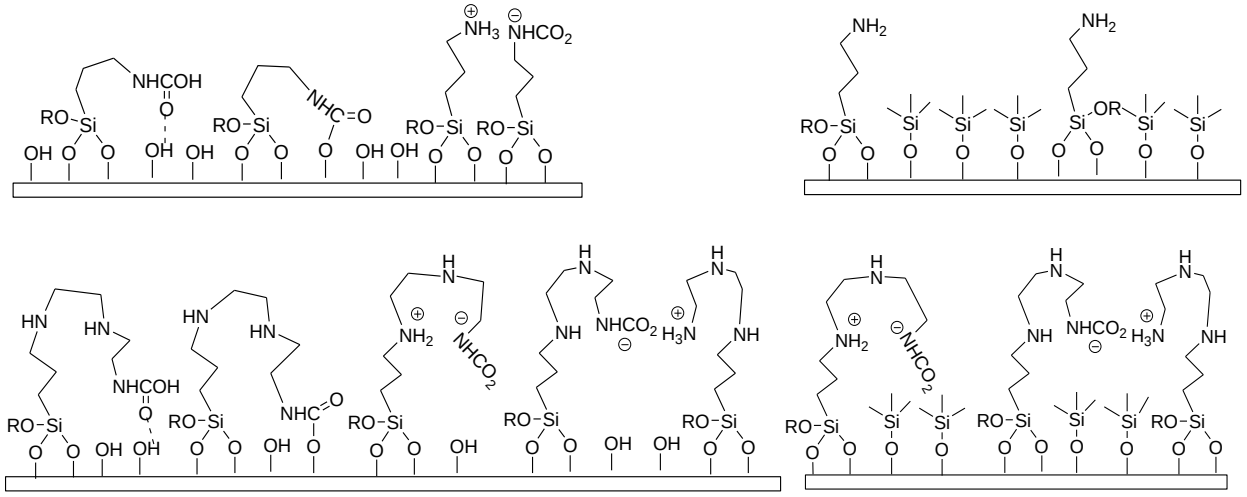

Figure 2.8. Schematic description of hypothesized species resulting from CO_2 chemisorption on organosilane modified silica adsorbents. MONO (top left), HMDS-MONO (top right), TRI (bottom left), HMDS-TRI (bottom right).

Other than the primary amine interactions with silanols on DI, TRI, and TREN samples, secondary amine interactions with surface silanol also available, but these species are not depicted on Figure 2.8. When two amine moieties interact to effect CO_2 adsorption, it has been shown previously that alkylammonium carbamate species are formed (see above).As mentioned above, since the longer silane chains offer more mobility and flexibility, these carbamate species can be formed primarily intermolecularly at high organosilane loadings, or intramolecularly at low organosilane loadings. The data above suggest that intramolecular species are more efficiently

formed by two amines separated by a distance of five atoms (i.e. on TRI and TREN), rather than two atoms, as may occur with adjacent amines on a DI, TRI or TREN chains, as shown in Figure 2.7. After capping of surface silanols (Figure 2.8, bottom right), even though alkylammonium carbamate species may still be formed with two amines in close proximity, carbamic acid species bonded to silanol groups via hydrogen bonds likely cannot be formed, as can be inferred from the lack of significant CO_2 uptake on HMDS-MONO.

Isosteric heats of adsorption

Figure 2.9 shows the isosteric heats of adsorption for the array of organosilane modified adsorbents along with of the corresponding CO_2 uptake. The bare SBA15 sample showed a heat of adsorption of 37 kJ/mol at close to zero CO_2 coverage, which corresponds to the isosteric heat of physisorption of CO_2 on surface silanols. Compared to the isosteric heat of adsorption of the bare SBA15 sample, the MONO adsorbent showed a moderately higher isosteric heat of adsorption of 46 kJ/mol at close to zero coverage. Alkhabbaz et al.[19] also measured similar isosteric heats of adsorption with a 3-aminopropyl silane (0.87 N mmol/g) modified silica adsorbent. The slightly higher amine loading in that work resulted in a sorbent with a modestly higher heat of adsorption than that measured for the MONO sample here. In the Alkhabbaz et al. work, we suggested that the observed heat of adsorption (higher than bare silica, lower than MONO materials with high amine loadings) was associated with the low probability of having two paired primary amines necessary for forming alkylammonium carbamate species at tested low amine loading. The nature of the adsorbed CO_2 in that case was not assigned, and in this work we suggest the CO_2 may be adsorbed via amine interactions with silanols. Considering the lower amine loading of the MONO adsorbent studied here (0.45 N mmol/g) and the similar CO_2 adsorption capacity for the HMDS-

MONO and HMDS-SBA15 materials, the increased isosteric heat of adsorption for MONO adsorbent might be mainly caused by amine-silanol interactions, as the possibility of intermolecular interactions between two adjacent primary amines appears to be negligible (Table 2.2). The HMDS-MONO adsorbent gave a modestly higher heat of adsorption (31 kJ/mol) than that of HMDS-SBA15 material (25 kJ/mol), which might be associated with different forms of physisorbed CO_2, or very limited intermolecular CO_2 capture by adjacent amines.

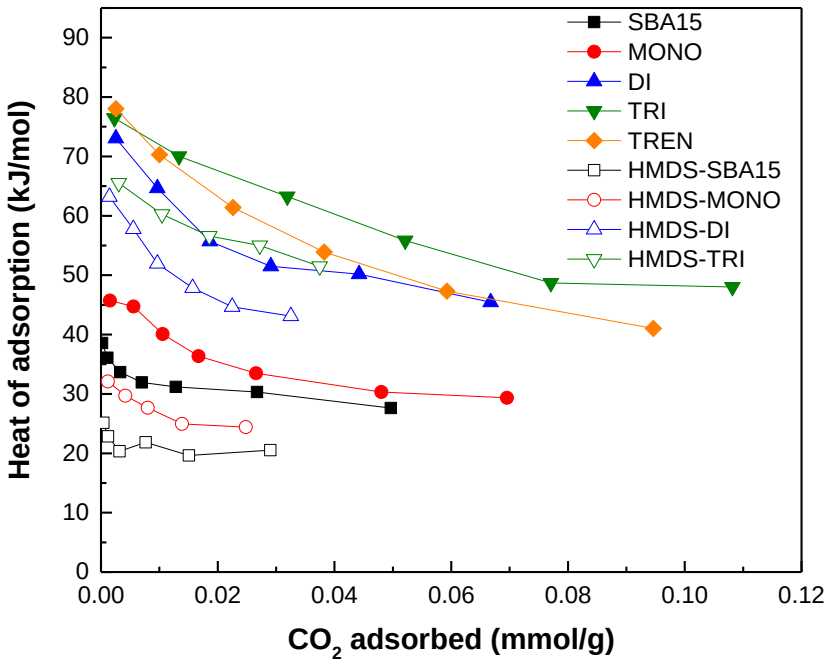

Figure 2.9. Isosteric heats of adsorption for uncapped (MONO, DI, TRI, and TREN) and capped (HMDS-MONO, -DI, -TRI) adsorbents, as well as the capped and uncapped bare silica supports.

The DI, TRI and TREN adsorbents showed relatively higher heats of adsorption (73-78 kJ/mol) compared to the MONO and bare silica materials at very low CO_2 surface coverages. These values are hypothesized to be associated with the combination of CO_2 adsorbed via amine-silanol and intramolecular amine-amine interactions. Since the surface energy of the HMDS adsorbents was changed after capping the silanols, as shown by the change of the heat of adsorption

for SBA15 and HMDS-SBA15, it was expected that the HMDS-DI and HMDS–TRI adsorbents would also analogously show lower heats of adsorption. This was indeed observed, with the HMDS-DI and HMDS–TRI adsorbents having heats of adsorption of 64-66 kJ/mol. As the CO_2 coverage on the surface of the adsorbent increased, the isosteric heat of adsorption of the DI adsorbent steeply decreased, while that of the TRI adsorbent was more gradually reduced. This trend also was observed with the HMDS–DI and HMDS–TRI samples. Belmabkhout et al.[12] calculated the heat of adsorption of a TRI modified silica adsorbent with high organosilane loading (2.63 mmol silane/g)[31] and showed that the slope of the heat of adsorption curve changed after a key CO_2 adsorption capacity (2.5 mmol CO_2/g). They argued that the CO_2 adsorption pattern changed from chemisorption to physisorption at this transition point. From this point of view, it is suggested that the domain of dominant physisorption of CO_2 for the DI adsorbent started at a lower CO_2 uptake compared to that of the TRI sample, which is supported by the data shown in Figure 2.6. While the slope of the CO_2 adsorption isotherm for the DI adsorbent changed around a loading of 0.035 mmol/g of CO_2, the TRI adsorbent showed a higher transition point of 0.09 CO_2 mmol/g. These data further suggest that cooperative, intramolecular adsorption occurs more readily on the TRI adsorbent.

2.4. Conclusions

To explore CO_2 adsorption capacity of isolated, single aminosilane molecules, four sorbents with low organosilane loadings (<0.45 silane mmol/g) were synthesized using an SBA15 support. An array of silanol-capped sorbents was prepared and tested, in parallel. The CO_2 adsorption isotherms were measured at low CO_2 pressures, and simultaneously, the isosteric heats of adsorption were measured via calorimetry. Each amine-containing sample showed a CO_2 uptake

that increased logarithmically at low pressures of CO_2 (chemisorption) and then increased linearly at higher pressures of CO_2 (physisorption).

The low silane loadings allowed analysis of the sorption data to infer if intramolecular CO_2 adsorption between two amine pairs was possible or probable in an intramolecular manner, using two amines in a single DI, TRI or TREN silane. Since possible cooperative amine pairs increased along with the number of amines in a single silane molecule, the silane molecule efficiency increased in the following order: MONO<DI< TRI<TREN. Upon removal of the silanols on the surface, the silane molecule efficiency of the HMDS-adsorbents decreased compared to the uncapped adsorbents. While the CO_2 uptake for the MONO adsorbent was higher than that of bare SBA15, the CO_2 uptake of the HMDS-MONO adsorbent was similar to that of HMDS-SBA15. From these results, the hypothesis that amine interactions with hydroxyl groups can yield CO_2 adsorption was supported, and removal of hydroxyls prevent the HDMS-MONO sorbent from chemisorbing CO_2, as its amines were isolated from each other, on average. The silane molecule efficiency of HMDS-DI was slightly higher than that of HMDS-MONO, but the HMDS-TRI sample had a much higher efficiency than the other HMDS samples. This suggests that the alkyl chain ($NH_2CH_2CH_2NH$) of the DI sample was not as effective at adsorbing CO_2 via NH_2-NH intramolecular interactions as for the TRI material.

The isosteric heats of adsorption of the various adsorbents allowed for initial assignments of the heats of adsorption to different hypothesized CO_2-surface interactions. The MONO adsorbent had a heat of adsorption of 46 kJ/mol at low CO_2 coverage, which was reduced to 31 kJ/mol on HMDS-MONO. This latter value may be considered as a heat of physisorption of CO_2 on the HMDS-SBA15 sample, whereas bare silica containing silanols gave a heat of adsorption of 37 kJ/mol (capped, bare silica was 25 kJ/mol). The sorption on MONO yielding a heat of 45 kJ/mol

was assigned to CO_2 sorption between an amine and a surface silanol. Sorption between two amines in a single silane chain, as is hypothesized to occur readily on TRI and TREN, gave a heat of adsorption of about 65 kJ/mol (HDMS capped) or higher 73-78 kJ/mol (silanol-containing). From this array of experiments on sorbents specifically synthesized to assess intramolecular CO_2 sorption, evidence has been gathered to support the hypothesis that such intramolecular sorption can occur on a single silane chain that contains multiple amines, a conclusion that could not be unambiguously asserted from prior studies of these silanes at high silane loadings.

2.5. References

(1) Dibenedetto, A.; Aresta, M.; Fragale, C.; Narracci, M. Reaction of Silylalkylmono- and Silylalkyldi-Amines with Carbon Dioxide: Evidence of Formation of Inter- and Intra-Molecular Ammonium Carbamates and Their Conversion into Organic Carbamates of Industrial Interest under Carbon Dioxide Catalysis. *Green Chem.* **2002**, *4* (5), 439–443.

(2) Zheng, F.; Tran, D. N.; Busche, B. J.; Fryxell, G. E.; Addleman, R. S.; Zemanian, T. S.; Aardahl, C. L. Ethylenediamine-Modified SBA-15 as Regenerable CO2 Sorbent. *Ind. Eng. Chem. Res.* **2005**, *44* (9), 3099–3105.

(3) Knowles, G. P.; Delaney, S. W.; Chaffee, A. L. Amine-Functionalised Mesoporous Silicas as CO2 Adsorbents. In *Nanoporous Materials IVProceedings of the 4th International Symposium on Nanoporous Materials*; Catalysis, A. S. and M. J. B. T.-S. in S. S. and, Ed.; Elsevier, 2005; Vol. Volume 156, pp 887–896.

(4) Knowles, G. P.; Delaney, S. W.; Chaffee, A. L. Diethylenetriamine [Propyl (Silyl)] - Functionalized (DT) Mesoporous Silicas as CO 2 Adsorbents. *Ind. Eng. Chem. Res.* **2006**, 2626–2633.

(5) Bacsik, Z.; Ahlsten, N.; Ziadi, A.; Zhao, G.; Garcia-Bennett, A. E.; Martín-Matute, B.; Hedin, N. Mechanisms and Kinetics for Sorption of CO 2 on Bicontinuous Mesoporous Silica Modified with N-Propylamine. *Langmuir* **2011**, *27* (17), 11118–11128.

(6) Dunne, J. A.; Mariwala, R.; Rao, M.; Sircar, S.; Gorte, R. J.; Myers, A. L. Calorimetric Heats

of Adsorption and Adsorption Isotherms. 1. O2, N2, Ar, CO2, CH4, C2H6, and SF6 on Silicalite. *Langmuir* **1996**, *12* (24), 5888–5895.

(7) Chakraborty, A.; Saha, B. B.; Koyama, S.; Ng, K. C. On the Thermodynamic Modeling of the Isosteric Heat of Adsorption and Comparison with Experiments. *Appl. Phys. Lett.* **2006**, *89* (17), 171901–171903.

(8) Cavenati, S.; Grande, C. A.; Rodrigues, A. E. Adsorption Equilibrium of Methane, Carbon Dioxide, and Nitrogen on Zeolite 13X at High Pressures. *J. Chem. Eng. Data* **2004**, *49* (4), 1095–1101.

(9) Furmaniak, S.; Terzyk, A. P.; Gauden, P. A.; Harris, P. J. F.; Kowalczyk, P. The Influence of Carbon Surface Oxygen Groups on Dubinin–Astakhov Equation Parameters Calculated from CO2 Adsorption Isotherm. *J. Phys. Condens. Matter* **2010**, *22*, 085003.

(10) Didas, S. A.; Kulkarni, A. R.; Sholl, D. S.; Jones, C. W. Role of Amine Structure on Carbon Dioxide Adsorption from Ultradilute Gas Streams such as Ambient Air. *ChemSusChem* **2012**, *5* (10), 2058–2064.

(11) Zukal, A.; Jagiello, J.; Mayerová, J.; Cejka, J. Thermodynamics of CO2 Adsorption on Functionalized SBA-15 Silica. NLDFT Analysis of Surface Energetic Heterogeneity. *Phys. Chem. Chem. Phys.* **2011**, *13* (34), 15468–15475.

(12) Belmabkhout, Y.; Sayari, A. Effect of Pore Expansion and Amine Functionalization of Mesoporous Silica on CO2 Adsorption over a Wide Range of Conditions. *Adsorption* **2009**, *15* (3), 318–328.

(13) Su, F.; Lu, C.; Kuo, S. C.; Zeng, W. Adsorption of CO2 on Amine-Functionalized Y-Type Zeolites. *Energy and Fuels* **2010**, *24* (2), 1441–1448.

(14) Yan, X.; Komarneni, S.; Yan, Z. CO2 Adsorption on Santa Barbara Amorphous-15 (SBA-15) and Amine-Modified Santa Barbara Amorphous-15 (SBA-15) with and without Controlled Microporosity. *J. Colloid Interface Sci.* **2013**, *390* (1), 217–224.

(15) Knöfel, C.; Descarpentries, J.; Benzaouia, A.; Zeleňák, V.; Mornet, S.; Llewellyn, P. L.; Hornebecq, V. Functionalised Micro-/mesoporous Silica for the Adsorption of Carbon Dioxide. *Microporous Mesoporous Mater.* **2007**, *99* (1-2), 79–85.

(16) Mello, M. R.; Phanon, D.; Silveira, G. Q.; Llewellyn, P. L.; Ronconi, C. M. Amine-Modified MCM-41 Mesoporous Silica for Carbon Dioxide Capture. *Microporous Mesoporous Mater.* **2011**, *143* (1), 174–179.

(17) Knöfel, C.; Martin, C.; Hornebecq, V.; Llewellyn, P. L. Study of Carbon Dioxide Adsorption on Mesoporous Aminopropylsilane- Functionalized Silica and Titania Combining Microcalorimetry and in Situ Infrared Spectroscopy. *J. Phys. Chem. C* **2009**, *113* (52), 21726–21734.

(18) da Silva, F. W. M.; Maia, D. S.; Oliveira, R. S.; Moreno-Piraján, J. C.; Sapag, K.; Cavalcante, C. L.; Zgrablich, G.; Azevedo, D. C. S. Adsorption Microcalorimetry Applied to the Characterisation of Adsorbents for CO2 Capture. *Can. J. Chem. Eng.* **2012**, *90* (6), 1372–1380.

(19) Alkhabbaz, M. A.; Bollini, P.; Foo, G. S.; Sievers, C.; Jones, C. W. Important Roles of Enthalpic and Entropic Contributions to CO2 Capture from Simulated Flue Gas and Ambient Air Using Mesoporous Silica Grafted Amines. *J. Am. Chem. Soc.* **2014**, *136* (38), 13170–13173.

(20) Danon, A.; Stair, P. C.; Weitz, E. FTIR Study of CO2 Adsorption on Amine-Grafted SBA-15: Elucidation of Adsorbed Species. *J. Phys. Chem. C* **2011**, *115* (23), 11540–11549.

(21) Moschetta, E. G.; Sakwa-Novak, M. A.; Greenfield, J. L.; Jones, C. W. Post-Grafting Amination of Alkyl Halide-Functionalized Silica for Applications in Catalysis, Adsorption, and 15N NMR Spectroscopy. *Langmuir* **2015**, *31* (7), 2218–2227.

(22) Kim, C.; Shah, B. P.; Subramaniam, P.; Lee, K. B. Synergistic Induction of Apoptosis in Brain Cancer Cells by Targeted Codelivery of siRNA and Anticancer Drugs. *Mol. Pharm.* **2011**, *8* (5), 1955–1961.

(23) Bollini, P. Amine-Oxide Adsorbents for Post-Combustion CO2 Capture, Ph.D. Thesis, Georgia Institute of Technology, 2013.

(24) Rezaei, F.; Sakwa-Novak, M. A.; Bali, S.; Duncanson, D. M.; Jones, C. W. Shaping Amine-Based Solid CO2 Adsorbents: Effects of Pelletization Pressure on the Physical and Chemical Properties. *Microporous Mesoporous Mater.* **2015**, *204*, 34–42.

(25) Aziz, B.; Hedin, N.; Bacsik, Z. Quantification of Chemisorption and Physisorption of Carbon

Dioxide on Porous Silica Modified by Propylamines: Effect of Amine Density. *Microporous Mesoporous Mater.* **2012**, *159*, 42–49.

(26) Ko, Y. G.; Shin, S. S.; Choi, U. S. Primary, Secondary, and Tertiary Amines for CO2 Capture: Designing for Mesoporous CO2 Adsorbents. *J. Colloid Interface Sci.* **2011**, *361* (2), 594–602.

(27) Didas, S. A.; Zhu, R.; Brunelli, N. A.; Sholl, D. S.; Jones, C. W. Thermal, Oxidative and CO2 Induced Degradation of Primary Amines Used for CO2 Capture: Effect of Alkyl Linker on Stability. *J. Phys. Chem. C* **2014**, *118* (23), 12302–12311.

(28) Brunelli, N. A.; Didas, S. A.; Venkatasubbaiah, K.; Jones, C. W. Tuning Cooperativity by Controlling the Linker Length of Silica-Supported Amines in Catalysis and CO2 Capture. *J. Am. Chem. Soc.* **2012**, *134* (34), 13950–13953.

(29) Bhagiyalakshmi, M.; Yun, L. J.; Anuradha, R.; Jang, H. T. Utilization of Rice Husk Ash as Silica Source for the Synthesis of Mesoporous Silicas and Their Application to CO2 Adsorption through TREN/TEPA Grafting. *J. Hazard. Mater.* **2010**, *175* (1-3), 928–938.

(30) Didas, S. A.; Sakwa-novak, M. A.; Foo, G. S.; Sievers, C.; Jones, C. W. Effect of Amine Surface Coverage on the Co-Adsorption of CO2 and Water: Spectral Deconvolution of Adsorbed Species. *J. Phys. Chem. Lett.* **2014**, *5*, 4194−4200.

(31) Serna-Guerrero, R.; Belmabkhout, Y.; Sayari, A. Further Investigations of CO2 Capture Using Triamine-Grafted Pore-Expanded Mesoporous Silica. *Chem. Eng. J.* **2010**, *158* (3), 513–519.

CHAPTER 3

CO_2 ADSORPTION ON AMINE FUNCTIONALIZED NANOCELLULOSE

3.1. Background

Microfibrillated cellulose (MFC) is a promising support material for CO_2 adsorbents, considering its abundance nature, strong mechanical properties and eco-friendliness. On top of that, the hydroxyl groups of MFC can be chemically modified by grafting agents, akin to what is done with hydroxylated surfaces of silica, which might be another advantage. However MFC has poor surface area and pore volume because of its macroporous structure.

Almost all CO_2 adsorbent support materials explored to date are metal oxides such as Al_2O_3, SiO_2, or activated carbon. Since a larger amount of amine molecules can be added to pores with higher surface areas and pore volumes, a number of researchers have used mesoporous silica supports such as SBA-15, MCM-41 and furthermore modified these support materials to increase their pore diameter. Harlick et al[1] expanded the pore diameter of MCM-41 from 3 nm to 13 nm and grafted 3-[2-(2-aminoethylamino)ethylamino]propyltrimethoxysilane on the oxide surface. Consequently, every key CO_2 adsorption criterion such as maximum CO_2 capacity, amine efficiency, and kinetics were improved. For these reasons, chiefly the success of mesoporous oxides, interest in MFC as an adsorbent support has been limited.

Meanwhile, Steinfeld et al.[2–5] recently reported amine functionalized MFC and its CO_2 capacity was competitive with other adsorbents based on amine modified inorganic supports. From their papers, even though the bare surface area of MFC was less than 25 m^2/g, the amine efficiency was 0.23, which suggested that the small surface area of the MFC was not a crucial drawback for its use as a CO_2 adsorbent support material. However, even though their papers provided the

possibility of usage of MFCs as supports for CO_2 adsorbents, the understanding of the physical structure and chemical properties of amine containing MFCs is additionally required to expand its application to different CO_2 adsorption materials.

First, as a class 1 material, a physical mixture of amine molecules (or polymers) with the MFC has not been reported, while nanocomposite materials with conventional polymer materials (c.a. PE[6], PP[7], PLA[8], PU[9], EVOH[10]) have been actively researched as structural materials. By mixing MFC with these polymer materials, their mechanical strength and chemical properties were enhanced. In these applications, MFC acted as a filler. However, the role of the MFC as a class 1 adsorbent support is providing space between amine molecules so that CO_2 molecules would be adsorbed without transport limitations. In general, in amine adsorbents, short amine containing molecules (c.a. DETA, TETA, TEPA) and branched amine polymer (c.a. PEI) are commonly used.

While class 1 adsorbents could be easily synthesized under mild conditions via an impregnation method, access to the impregnated amine molecules in the adsorbent during the cyclic operation of CO_2 adsorption and desorption has been considered a major drawback. Thus, research on class 2 materials also consistently has attracted attention because amine molecules are covalently grafted on the surface, and typically do not fill and clog the pores. Mainly, class 2 materials have been prepared using amine containing silane molecules that were hydrolyzed and condensed with hydroxyl groups of the pre-synthesized support material, or the silanes were added to support precursors and they were co-condensed together. To date, inorganic supports have been widely used such as silica or alumina because hydroxyl groups are exposed on the surface of these materials and organosilanes are easily grafted on the hydroxyl groups via hydrolysis and condensation reactions.

As mentioned above, MFC may also be used as class 2 material supports because it contains

numerous hydroxyl groups that can likely be grafted with organosilanes. Cellulose is biopolymer that consists of a lot of glucose monomers, in which three free hydroxyl groups are connected to C2, C3 and C6. Compared to hydroxyl groups of inorganic supports, the reactivity of these hydroxyl groups on cellulose differ according to the carbon number. Even though several researchers have tried to exploit the differences in reactivity between the primary hydroxyl group at C6 and secondary hydroxyl groups at C2 and C3, their reactivity with organosilanes is still somewhat ambiguous because of the complex hydrogen bonding within cellulose chains.[11] On top of that, the reactivity of hydroxyl groups of various inorganic supports (Al_2O_3 or SiO_2) to organosilanes might be different, so the grafting yield (loaded Si/Added Si) also is affected by the material as well.

The grafting yield of these organosilanes is affected by various factors such as the grafting temperature, time, pH and the amount of water added.[12–14] However, because these organosilanes are easily hydrolyzed in water, most grafting processes are conducted under anhydrous conditions (anhydrous toluene) or with a small amount of water in a solvent to increase the grafting yield. However, applying the same preparation methods developed for oxide supports to handle MFC is challenging. Since the cellulose fiber is flexible and hydrophilic because of the surface hydroxyl groups, the fibers are agglomerated in nonpolar solvents. Indeed, hydroxyl groups in toluene solvent do not participate in grafting reactions. For this reason, MFC is usually functionalized in a polar solvent mixture (c.a. water/ethanol, water/acetone), but there is a limitation when these solvents are dried by freeze drying. To yield a higher porosity and surface area with cellulose materials, freeze drying is commonly used but the temporarily frozen solvent mixtures easily melt during the drying process because the freezing point of these solvent mixtures is much lower (ethanol :-114 ^{o}C, acetone: -95 ^{o}C) than pure water. Consequently, the only feasible solvent is water.

However, as mentioned above, the hydrolysis and condensation rates of amine containing silanes are quite fast in aqueous media, so homogeneous grafting on the MFC is very difficult to achieve. On top of that, since the reactivity of the various hydroxyls is different, controlling the grafting degree is a huge challenge.

In this research, class 1 and class 2 CO_2 adsorbents were synthesized with MFC supports. For class 1 materials, a conventional branched polymer, PEI, and a rarely researched (for CO_2 sorption) short branched amine molecule, tris(2-aminoethyl)amine (TREN), were physically impregnated into the MFC. In the case of class 2 materials, various amounts of two different organosilanes, 3-aminopropyltriethoxysilane and 3-aminopropyldiethoxymethylsilane, were grafted onto a MFC support and the CO_2 capacities of these adsorbents were evaluated. CO_2 uptakes were measured at a CO_2 concentration (400 ppm) consistent with capture from ambient air under the dry conditions and the bulk textural properties of the adsorbents were assessed with SEM images. The molecular level structure of the poly(siloxane) species were analyzed by solid state CP-MAS ^{29}Si NMR and ex-situ FTIR. The chemisorbed CO_2 species on the organosilane functionalized MFC were detected by in-situ FTIR after dosing 10 mbar of CO_2 over 8 h at 27 ^{o}C.

From the comparison of the CO_2 uptake of the new class 1 adsorbents, TREN/MFC and PEI/MFC, with reference adsorbents, TREN/SBA15, PEI/SBA15, the compatibility of MFCs as a class 1 support material was evaluated. The differences in physical and chemical aspects between dialkoxysilane and trialkoxysilane modified MFCs (class 2 materials) showed the potential cause for the enhanced CO_2 adsorption capacity of dialkoxysilane modified materials. Furthermore, the results from this study may provide the initial components of application guidelines for organosilane modification of cellulose nanomaterials.

3.2. CO_2 adsorption for amine impregnated MFC (Class 1)

3.2.1. Experimental

Materials

All chemicals (higher than Reagent Grade purity) were used without further purification. Tris(2-aminoethyl)amine (TREN), poly(ethyleneimine) (PEI, Mw ~800, Mn~600) and ethanol were purchased from Sigma-Aldrich. Micro-fibrillated cellulose (MFC) was purchased from the Process Development Center of the University of Maine as a slurry (2.8 wt. %). SBA15 support was synthesized as described in Chapter 2.

Impregnation of amine molecules in MFC

First, 18 g of MFC hydrogel (2.8 wt.%) was diluted with 30 g of DI water to yield 1 wt. % of MFC hydrogel and the slurry was stirred for 3 h at room temperature. Then, 0.214 g or 0.333 g (30 or 40 wt. % as an adsorbent base) of TREN or PEI were added to the mixture and vigorously stirred for 3 h. The amine containing MFC mixture was poured into a centrifuge tube and was immersed in the liquid nitrogen for 15 min. The water in the frozen mixture was removed by a freeze dryer (Freezone 6, Labcono) at -55 °C under the 0.4 mbar of pressure for 2 days. The final adsorbents were named based on the nominal amine contents in the adsorbent, such as TREN40/MFC, PEI40/MFC.

Impregnation of amine molecules in SBA15

As reference samples, the same amount of amine molecules (TREN and PEI) were impregnated into porous silica using the following procedure. First, 0.333 g (40 wt. % as an

adsorbent base) of TREN or PEI were fully dissolved in 50 mL of ethanol. Then, 0.5 g of pre-synthesized, dried SBA15 was added into the amine containing ethanol solution. The mixture was stirred for 3 h and the ethanol solvent was removed by rotary evaporation. The product was dried overnight at 60 ^{o}C under the 10 mmHg of pressure. Similarly, the amine impregnated SBA15 materials were named as TREN40/SBA15 and PEI40/ SBA15

Characterization

The specific surface areas and pore volumes of the adsorbents were calculated or measured from nitrogen physisorption isotherms obtained at 77 K (Tristar II 3020, Micrometrics). Before each analysis, the samples were degassed under 20 mTorr of pressure at 120 °C for 12 h. The specific surface areas of the adsorbents were calculated by the BET method. Elemental compositions were measured at Atlantic Microlab (Norcross, GA). N analysis was performed by combustion using an automatic analyzer. All samples were dried at 60 °C under -0.015 mmHg of vacuum prior to measurement. SEM images were taken on a Hitachi SU8010 at an accelerating voltage of 5 kV. Samples were prepared by depositing on an SEM sample holder and then gold coating with gold sputtering (Q150T, Quorum). The functional groups of bare MFC and amine modified MFC were identified with a Bruker Vertex 80V infrared spectrometer operating in ATR mode in the range of 400-4000 cm^{-1}. The samples were torn down to small pieces (~ 1cm x 1 cm) and placed on the plate of the Platinum ATR. All spectra were recorded with 64 scans at room temperature. The dry CO_2 adsorption capacities of amine modified MFCs were measured by TGA (Q500, TA Instruments) analysis under a flow (90 mL/min) of 400 ppm of CO_2 with He balance. About 20 mg of sample was placed on the platinum holder and pretreated under an He atmosphere at 120 ^{o}C for 3 h. After cooling to 25 ^{o}C, the temperature was maintained for 1 h under He flow, then the sample was exposed to 400 ppm of CO_2 for 6 h.

3.2.2. Results and discussions

Physical properties of amine impregnated adsorbents and bare supports

The surface areas, pore volumes and amine loadings of the adsorbents are listed in Table 3.1. The surface area of unmodified MFC was 25 m^2/g, which is extremely small compared to the surface area of SBA15 (799 m^2/g). The pore volume of the MFC was also negligible (0.05 cm^3/g). Since the structure of MFC consists of only macropores and some of the microfibrillated fibers are agglomerated during the freeze drying process, a low surface area and pore volume were obtained. Furthermore, the porosity and surface area values were not measurable for the amine impregnated (class 1) MFC adsorbents. On the other hand, 40wt. % of PEI impregnated SBA15 adsorbents showed 95 % of pore filling (0.95 $cm^3/g \rightarrow 0.04$ cm^3/g) and reduction of the surface area. (799 m^2/g $\rightarrow$ 20 m^2/g) while TREN40/SBA15 showed 0.10 cm^3/g of pore volume and 38 m^2/g of surface area. From the elemental analysis of the adsorbents, evaporation of TREN from both the MFC and silica based adsorbents was observed during the heating treatment prior to CO_2 adsorption analysis, as verified by measuring the amine loading before and after the heat treatment. The values in parenthesis are the amine loading after the 120 ^oC heat treatment for 2 h. In the case of PEI modified adsorbents, there was no noticeable amine loading change. The higher surface area and pore volume of TREN40/SBA15 than PEI40/SBA15 might be a result of the evaporation of TREN during the degassing process.

Table 3.1. The surface areas, pore volumes and amine loadings of PEI or TREN impregnated adsorbents.

Samples	Amine loading (N mmol/g)	Surface area (m^2/g)	Pore volume (cm^3/g)
MFC	0	25	0.05
PEI30/MFC	8.60	Not measurable	Not measurable
PEI40/MFC	10.95	Not measurable	Not measurable
TREN30/MFC	8.20 (6.35)[a]	Not measurable	Not measurable
TREN40/MFC	10.94 (8.18)	Not measurable	Not measurable
SBA15	0	799	0.95
PEI40/SBA15	11.4	20	0.04
TREN40/SBA15	10.72 (8.6)	38	0.10

[a] The values in parenthesis are the amine loading after 120 ^oC heat pretreatment (2 h) in the TGA-CO_2.

Weight changes during heating pretreatment

The weight changes of pure TREN and the amine impregnated adsorbents were measured by TGA analysis. Figure 3.1 (left), shows the weight change of pure TREN along with the programmed temperature profile. To determine the amount of evaporation of TREN during the pretreatment before CO_2 dosing in the TGA (120 ^oC, 2 h, He flow), the temperature was increased to 120 ^oC for 30 min and maintained for 2 h, then the temperature was increased to 900 ^oC with 10 ^oC/min ramp speed to check the decomposition temperature of TREN. When the temperature reached 120 ^oC, the weight of TREN began to reduce, which indicates that TREN is evaporated at this temperature. Even though the boiling point of TREN is 265 ^oC at 1 bar, because of the high volatility of TREN at 120 ^oC, 80% of pure TREN was evaporated during 2 h, and when the temperature reached 600 ^oC, all of the TREN was decomposed or evaporated. Figure 3.1, right,

shows the weight change of the adsorbents during pretreatment prior to CO_2 adsorption analysis via TGA. Under the assumption that the evaporation of TREN was negligible below 120 ^oC, as shown Figure 3.1 (left), the weight change between 25^oC to 120 ^oC for 30 min was assumed as evaporation of water or bound CO_2. Similar weight changes (12-19 wt.%) were shown form every adsorbent during the first 30 min of pretreatment (25 ^oC → 120 ^oC). Relatively, the MFC support would tend to adsorb more water (16-19 wt. %) than the SBA15 support. (12-13 wt. %). However, huge differences in weight changes during the 120 ^oC temperature hold region were observed between TREN or PEI modified adsorbents. While PEI40/MFC and PEI40/SBA15 showed less than 2 wt. % of weight changes, TREN40/MFC and TREN40/SBA15 lost 16 wt% of TREN. These results are consistent with the amine loading changes before and after heating treatments, as shown in Table 3.1, and are due to the relative volatility of TREN.

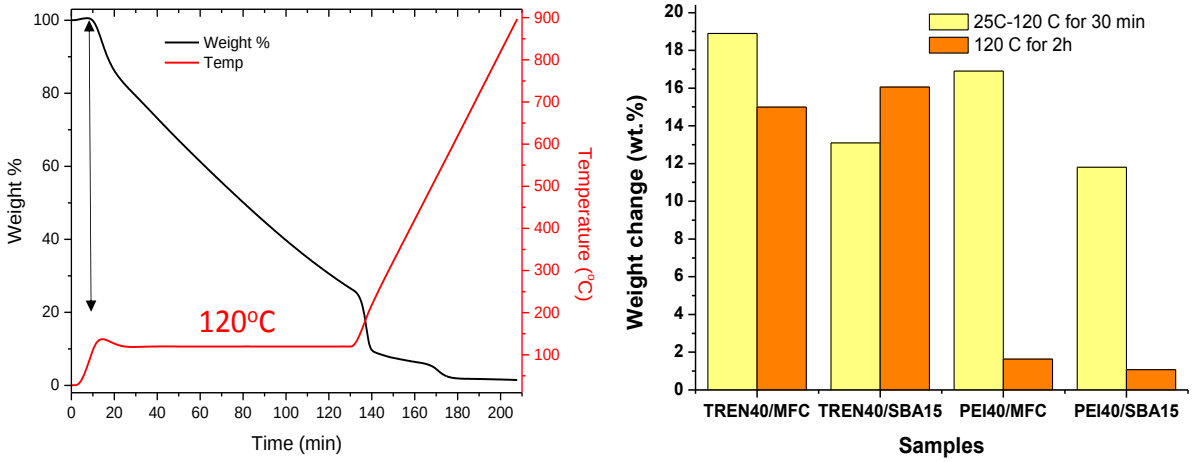

Figure 3.1. (left) Weight change of pure TREN along with the temperature profile and (right) TREN or PEI impregnated adsorbents during 30 min of heating (25 ^oC → 120 ^oC) and 2 h of soaking (120 ^oC).

CO_2 adsorption for amine impregnated MFC

The CO_2 uptakes and amine efficiencies for PEI30/MFC, PEI40/MFC, PEI40/SBA15, and TREN40/SBA15, along with the adsorption times, are shown in Figure 3.2. Interestingly, TREN30/MFC and TREN40/MFC barely adsorbed any CO_2, thus their CO_2 uptakes are not depicted in Figure 3.2. As soon as the other adsorbents were exposed to 400 ppm CO_2/He, the CO_2 uptakes were steeply increased in a few minutes and then slowly increased to a steady state point. Since the adsorption time (6 h) was not enough to reach a true equilibrium steady state, the comparison of the CO_2 uptake rate cannot be quantitatively explained based on the ratio of CO_2 uptake (time) / total CO_2 uptake at steady state. However, it can be observed that the CO_2 uptake rate for the SBA15 adsorbents was relatively faster than that of the MFC adsorbent when considering the slope of the uptake in figure 3.2 (left) before 50 min. Furthermore it can be inferred that the TREN40/SBA15 and PEI40/SBA15 would likely reach steady state in a shorter time than the PEI/MFC adsorbents, which can be interpreted as the fast adsorption kinetics for the SBA15 adsorbents originated from the ordered mesoporous structure of the SBA15, as shown in chapter 2, Figure 2.2. On the other hand, MFC adsorbents consist of disordered macro pore structures, which will be shown later. The amine efficiencies of the adsorbents are shown in Figure 3.2 (right), which are calculated based on the remained amine loadings after 2 h of heating treatment. As the PEI loading on the MFC increased, the amine efficiencies also increased, which indicates that a larger number of amines are participating in capturing CO_2. Even though the amine efficiency of PEI40/MFC (0.079) was lower than PEI40/SBA15 (0.091) at 500 min of adsorption time, considering the extremely small surface area of the support, the MFC could be a promising support material for CO_2 adsorption using PEI. In the case of TREN40/SBA15, because of the evaporation of TREN during the pretreatment process, the pore volume might not be as filled with amines as

PEI40/SBA15, so the amine molecules were not close enough to effectively capture CO_2. Thus, the reduced intermolecular interactions might result in the lower amine efficiency observed for TREN40/SBA15 than PEI40/SBA15. However, the negligible CO_2 uptake observed for TREN30/MFC and TREN40/MFC cannot be easily explained because at the same TREN loading sample, TREN40/SBA15, showed reasonable amine efficiency (0.07, 500 min).

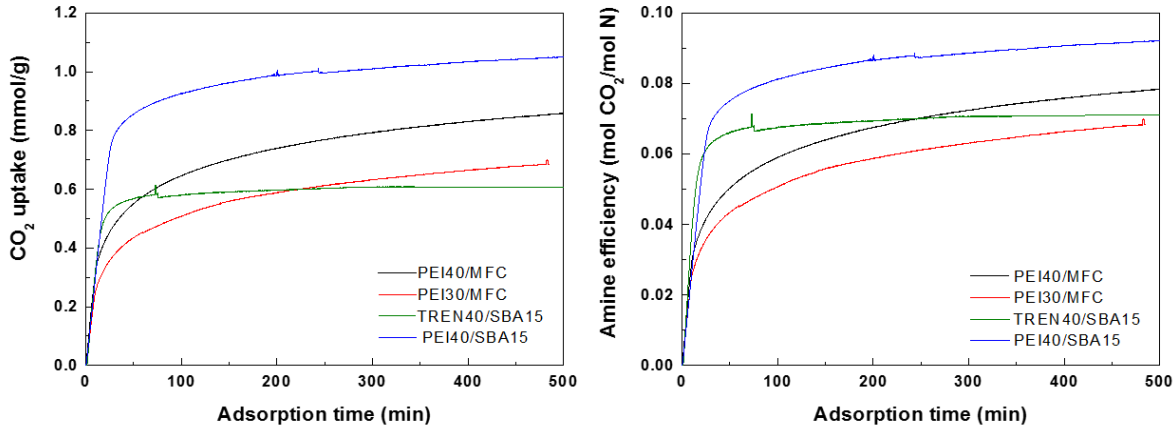

Figure 3.2. (left) CO_2 uptakes and (right) amine efficiencies for PEI or TREN impregnated adsorbents along with the CO_2 adsorption time

SEM images of amine impregnated MFCs

SEM images of PEI and TREN impregnated adsorbents and bare MFC are given in Figure 3.3. As mentioned above, MFC consists of macropores between irregular, cellulose nanofibers. Because of the freeze drying method employed in their preparation, fluffy fibril textures were developed. However, as the amine loading increased, agglomeration of the fibers was observed and the trend was more prominent for the TREN/MFC samples. As can be seen in the figure 3.3, the diameter of the fibers for the TREN40/MFC was significantly increased to 30 μm and a "bulk" TREN/cellulose mixture was formed. Compared to nano-sized diameters of the fibers from

unmodified MFC, the diameters of the fibers of the PEI/MFC adsorbents were also somewhat increased, but they still maintained their original fibril structures.

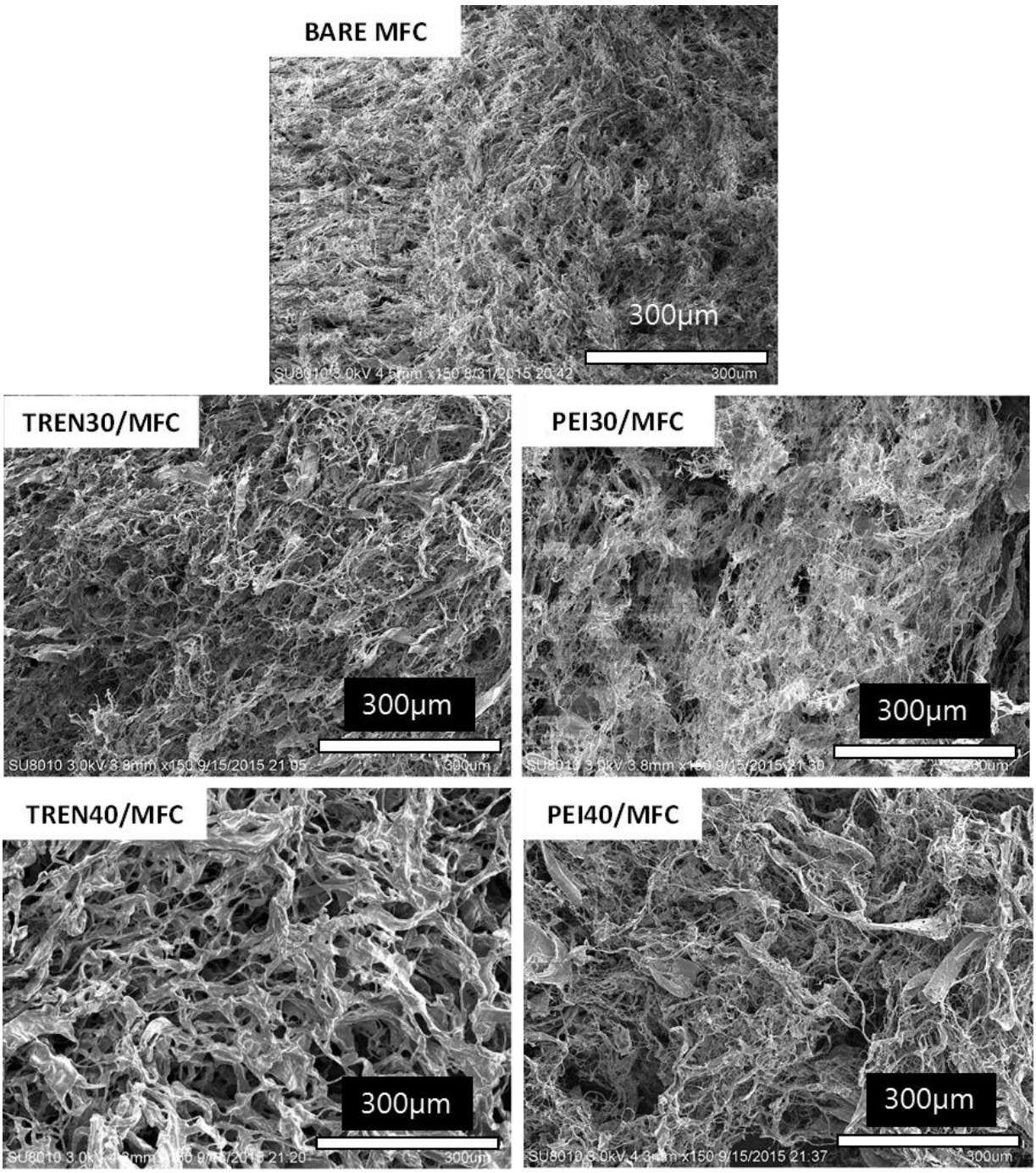

Figure 3.3. SEM images of PEI and TREN impregnated adsorbents, along with the bare MFC.

Hypothesized mechanism of thickening of fibers of TREN/MFCs

As shown in the SEM images of TREN40/MFC and PEI40/MFC, a remarkable difference in the structures of the two adsorbents can be seen when examining the diameter of the fibers. Under the assumption that primary amines of TREN or PEI can interact with the hydroxyl groups of MFCs via hydrogen bonding, the TREN and PEI molecules may locate between two fibers of the MFCs (Figure 3.4). While the MFC hydrogel and amine molecules were stirred in the flask during the synthesis of the composite materials, a new sub-block structure, fiber/TREN/fiber or fiber/PEI/fiber, may be stabilized via hydrogen bonding, and these sub-blocks might stick together between ice crystals while the hydrogel mixture was frozen. Since the size of TREN is quite small, it might effectively act as a binder between adjacent fibers and consequently form a more bulk-like cellulose fiber. On the other hand, the branched structure of PEI might provide enough space between two adjacent fibers such that they cannot be easily agglomerated during the freeze drying process. From this point of view, the primary amines of TREN and PEI also could interact with silanols on the SBA 15 support, but since their pore surfaces are rigid, the surface of SBA15 cannot be made mobile. Consequently, it can be suggested that TREN molecules were well dispersed on the surface of SBA15 and primary amine interactions with silanols cannot change the sorbent structure. Thus, reasonable CO_2 uptake from TREN40/SBA15 was observed because many amine molecules in TREN remain accessible, while TREN40/MFC did not adsorb CO_2 likely because most or all of the TREN molecules may have been embedded in the cellulose fibers and primary amines might be occupied by hydrogen bonding. However, to verify this hypothesis, further research is required, such as removing hydroxyl groups of MFC through surface modification methods before impregnation of amine molecules.

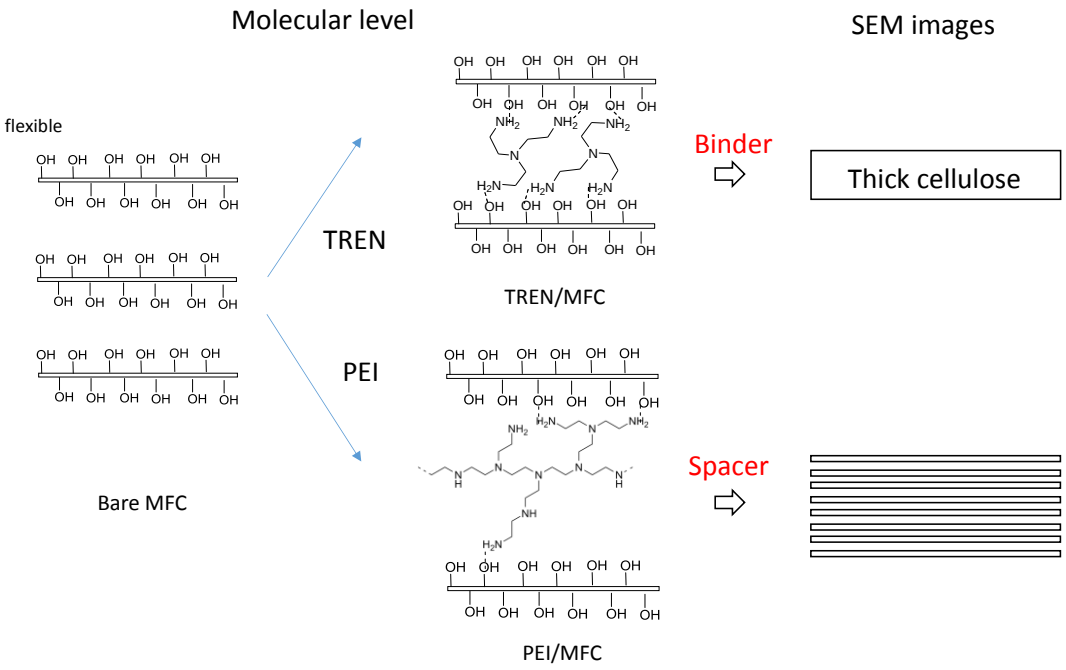

Figure 3.4. Hypothesized process for thickening the diameter of TREN or PEI impregnated MFCs.

3.3. CO_2 adsorption for organosilane modified MFC (Class 2)

3.3.1. Experimental

Materials

All chemicals (higher than Reagent Grade purity) were used without further purification. 3-aminopropylmethyldiethoxysilane (APDES), 3-aminopropyltriethyoxysilane (APTES) were purchased form Gelest. Micro-fibrillated cellulose (MFC) was purchased from the Process Development Center of the University of Maine as a slurry (2.8 wt. %)

Grafting of APTES and APDES on MFC

First, 1.8 g of MFC hydrogel was dispersed in 30 mL of DI water and stirred for 2 h. Various amounts of APTES (0-5 mmol N/g) or APDES (0-15 mmol N/g) were dropwise added to the diluted MFC hydrogel and stirred for 24 h. The mixture was poured into a centrifuge tube and immersed in liquid nitrogen for 15 min. The water in the frozen mixture was removed with a freeze dryer (Freezone 6, Labcono) at -55 °C under the 0.4 mbar of pressure for 2 days. The product was heated at 100 °C under the vacuum for 3 h. The final adsorbents were named based on the added amount of organosilanes per 1 g of bare MFC (dry) (c.a. 1 mmol of APDES to 1g of MFC = APDES 1) In the case of adsorbents films used for in-situ FTIR analysis, the mixture of the organosilane and the MFC hydrogel was spread on the glass plate and dried at room temperature for 2 days.

Characterization

The specific surface areas and pore volumes of the adsorbents were measured from

nitrogen physisorption isotherms at 77 K (Tristar II 3020, Micrometrics). Before each analysis, samples were degassed under 20 mmHg of pressure at 120 °C for 12 h. The specific surface areas of the adsorbents were calculated by the BET method and the pore size distributions were analyzed with the BJH method. The elemental composition was measured at Atlantic Microlabs (Norcross, GA). N analysis was performed by combustion using an automatic analyzer. All samples were dried at 100 °C under -0.015 mmHg of vacuum prior to measurement. The chemical structure of the organosilanes on the MFCs was verified by ^{29}Si-NMR spectroscopy. Cross polarization magic angle (CP-MAS) NMR spectra were collected with a Bruker DSX 300 MHZ equipped with 7 mm zirconia rotors. SEM images were taken on a Hitachi SU8010 at an accelerating voltage of 5 kV. Samples were prepared by depositing sample on an SEM sample holder and then gold coating with gold sputtering (Q150T, Quorum). The functional groups of bare MFC and amine modified MFC materials were identified with a Bruker Vertex 80V infrared spectrometer operating in ATR mode in the range of 400-4000 cm^{-1}. The samples were torn off to small pieces (~1 cm x 1 cm) and placed on the plate of the platinum ATR. All spectra were recorded with 64 scans at room temperature. The dry CO_2 adsorption capacities of the amine modified MFCs were measured by TGA (Q500, TA Instruments) analysis under a flow (90 mL/min) of 400 ppm of CO_2 and He balance. About 20 mg of sample was placed on the platinum holder and pretreated under a He atmosphere at 120^{o}C for 3 h. After cooling to 25^{o}C, the temperature was maintained for 1 h under He flow, and then the samples were exposed to 400 ppm of CO_2 for 6 h.

In-Situ FTIR for CO_2 species on the amine modified MFC

The adsorbed CO_2 species on the amine modified MFC were verified with in-situ FTIR. For this analysis, the film was loaded in the vacuum cell holder, which was mounted with a heater

and thermocouple. The film was dried under the vacuum at 120 °C for 3 h. When the temperature cooled to room temperature and the vacuum level stabilized below than 2.6 x 10^{-5} bar, spectra of the film were recorded as a background signal. Then 10^{-2} bar of CO_2 was dosed into the IR cell. From the dosing point, spectra were recorded every 2 min in the range of 400-4000 cm^{-1} with 64 scans at 27 °C.

3.3.2. Results and discussions

Post heat treatment for permanent covalent bond of Si-O-cellulose linkage

Compared to conventional functionalization of hydroxyl groups of metal oxides with organosilanes (silylation), grafting of organosilanes on the MFC requires one more step. In general, aqueous solvent systems are used for hydrolysis and condensation of organosilanes in the MFC hydrogel mixture. The water has to be removed for the completion of the condensation process, but the water is not perfectly removed and organosilanes are just connected to hydroxyl group of MFC via hydrogen bonding. Without a post condensation process, these loosely connected silanes are easily removed by filtration or centrifugation.[15] Thus, organosilane modified MFC needs to be heat treated after the freeze drying process or room temperature drying process for covalent bonds to be created between the silane and the MFC.

SEM images for organosilane grafted MFC

SEM images of bare MFC and APDES or APTES modified MFCs are shown in Figure 3.5 As noted in the above section, the bare MFC consists of irregularly aggregated cellulose fibrils, which results from ice crystal growth during freezing in liquid nitrogen. Under the dispersion condition of fibers in solvent, when the water is frozen, adjacent fibers are stuck together and dried.

Thus, the freezing technology for nanocellulose functionalization is an important factor for the final structure of the material. To freeze the MFC gel uniformly, Steinfeld et al. used a thin (3 mm) metal mold for freeze drying. However, this factor is not considered here and the only variable factors I explored was the nature of the organosilanes and the organosilane loading. If the MFC hydrogel were uniformly frozen with the metal mold, a more homogenous fiber structure could be obtained.[2] The bare MFC in this work shows a fluffy texture, as shown in Figure 3.5 (a), but as the APDES loading was increased, the void areas were filled with condensed organosilanes (Figure 3.5, b-d). Fluffy fiber structures thus changed to sheet structure and macro pores were eliminated. During the freezing process, the hydrolyzed silanes are located between ice crystals with cellulose fibers, and consequently a silane and fiber combined sheet structure was formed. As the silane loading increased, the sheet structure became more noticeable for both APDES and APTES modified MFCs. However, these sheet structure were more prominent for the APTES samples. While APDES 1 showed a similar fluffy fiber structure as the bare MFC, the same silane loading of APTES, giving APTES 1, showed already a well-developed sheet structure. As the APTES loading increased, the sheet structures were not further developed, but locally, a huge lump of material, hypothesized to be organosilane, was observed and the overall structure was irregular, as shown in Figure 3.5 (h), while the fiber diameter remained similar to APTES 1.

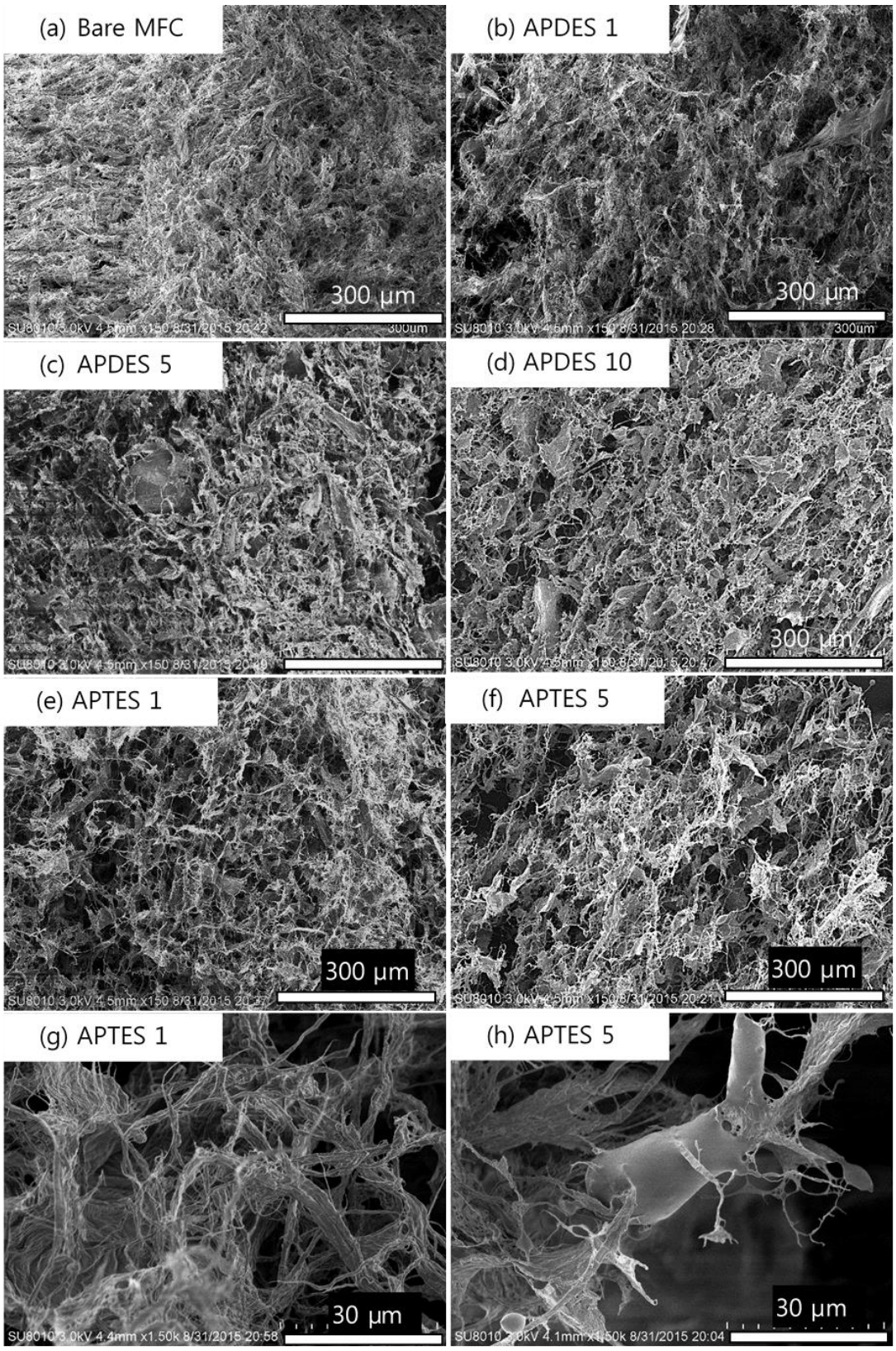

Figure 3.5. SEM images of MFC modified with various amounts of APDES or APTES.

CO_2 adsorption for organosilane grafted MFCs

Figure 3.6 shows the CO_2 adsorption uptake (black lines) and amine efficiencies (red lines) of amine functionalized MFCs. The amine efficiencies were calculated by dividing the CO_2 uptake with the amount of grafted amine on the adsorbent. APDES modified MFCs showed a steep increase in the CO_2 uptake with increasing amine loading. When 4.97 mmol/g of APDES was grafted on the MFC, the largest CO_2 uptake, 0.9 mmol CO_2/g, was observed (APDES-10), but the highest amine efficiency was observed by APDES 8.9 (0.185). Considering the surface area, pore volume and SEM images of the APDES modified MFCs, too large an amount of APDES (>8.9 mmol N/g) on the MFC filled the pores and blocked the CO_2 accessible paths to the amines, so that the amine efficiency decreased. On the other hand, the CO_2 uptake of APTES modified MFCs did not increase as much as for the APDES samples.

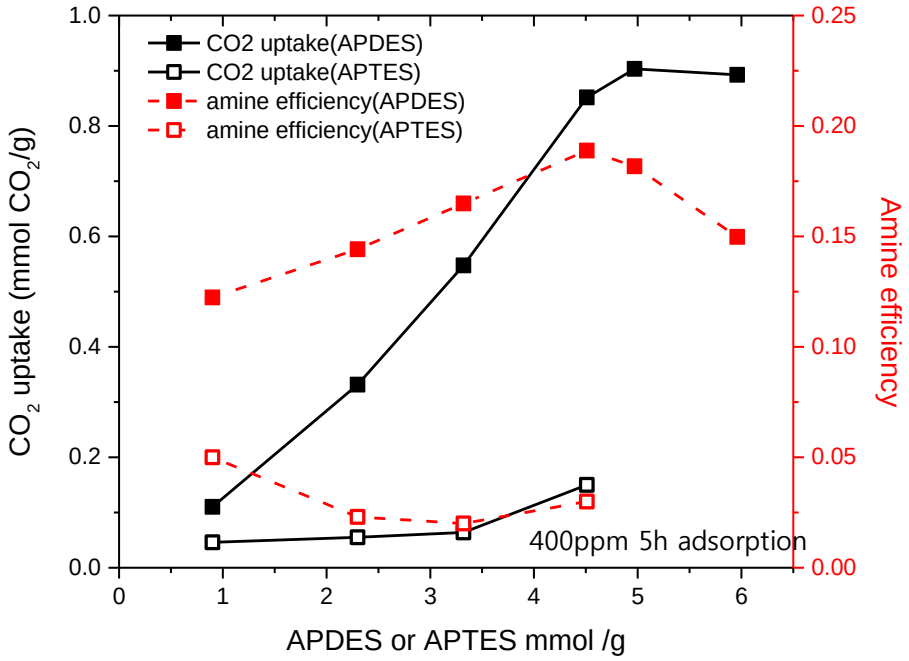

Figure 3.6. CO_2 uptakes and amine efficiencies for APDES or APTES modified MFCs.

Even though amine loadings of the APTES samples were similar to those of the APDES samples, the CO_2 uptakes of the APTES samples were extremely low and the amine efficiencies of the APTES samples did not exceed 0.05. APDES-10 showed almost 5 times higher of CO_2 adsorption capacity than APTES 8.3. This huge difference was a unique property of the surface of the MFC, which has not been shown with inorganic supports such as SBA15 or MCM41 silicas (APDES5/SBA15: 0.193 mmol CO_2/g, APTES5/SBA15: 0.156 mmol CO_2/g).

^{29}Si solid state NMR of APDES 5 and APTES 5

To elucidate the structure of organosilane on the MFCs, CP-MAS ^{29}Si NMR spectra of APDES5 and APTES5 were collected. In general, the chemical shifts of silicon are categorized as four types, M, D, T, and Q, which are named according to the number of alkoxy groups (OR) attached to the silicon atom. For example, structures of M, D, and T units can be express as: $R_1R_2R_3$-Si-(OR), R_1R_2-Si-$(OR)_2$ and R_1-Si-$(OR)_3$, respectively. These units can be made more specific by the number of alkoxy groups connected to different Si atoms, which are conventionally noted as M^n, D^n, T^n and Q^n. Figure 3.7 describes the probable poly(siloxane) structures of APDES or APTES modified MFCs. D^1 and T^1 represent chain-end silicon atoms, and D^2 and T^2 are linear sequence units. Since the APDES molecule has two alkoxy groups on the Si atom, linear poly(siloxane) structures might be formed on the surface of MFCs. T^3 can be shown for poly(siloxane) structure of the APTES adsorbents, which can be built as a three-dimensional network structure.

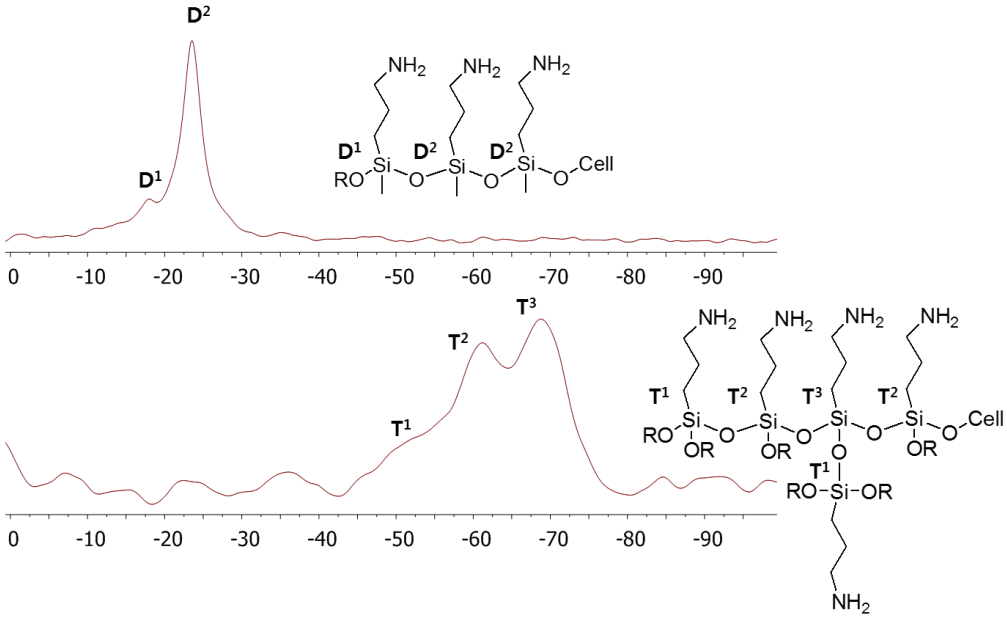

Figure 3.7. The probable poly(siloxane) structures of APDES (top) or APTES (bottom) modified adsorbents and solid state CP-MAS ^{29}Si NMR spectra of APDES 5 and APTES 5.

The CP-MAS solid state ^{29}Si NMR spectra of APDES 5 and APTES 5 are also shown in Figure 3.7. The spectrum of APDES 5 shows two peaks at -17, and -23 ppm, corresponding to D^1 and D^2 species, respectively. Considering that the predominant peak was shown at -23 ppm, a linearly polymerized poly(siloxane) chain might be grafted on the surface of the MFC, as shown in Figure 3.7. Since the chemical shifts of Si-O-C and Si-O-Si are categorized in the same D^2 shift and the signals of these linkages were not discriminated in Figure 3.7 (top), one cannot be verify the number of organosilanes polymerized in a single chain. APTES 5 shows 3 peaks at -50, 60 and 70 ppm, corresponding to T^1, T^2 and T^3 species, respectively. Since the intensity order of the peaks was $T^3>T^2>T^1$, it is suggested that the poly(siloxanes) in APTES 5 form a three dimensional, interconnected bulky structure. The peak of starting precursors for APDES (D^0) and APTES (T^0) were not observed because the rate of hydrolysis and condensation of silanes were accelerated by using DI water as a solvent.

FTIR spectra of organosilane grafted MFC

Figure 3.8 shows the FTIR spectra of the bare, ungrafted MFC. The inset of the figure represents the monomer structure of cellulose, which consists of 6 carbons, 6 oxygens and 10 hydrogens. As shown in the inset, the ring structure consists of five carbons (1-5) and one oxygen, with C6 connected to C5. C1 and C4 are connected to other cellulose monomers via β-glucosidic linkages. C2 and C3 contain hydroxyl and hydrogen groups in a trans-configuration. The FTIR spectrum of the bare MFC showed conventional bands for cellulose, such as a broad band of OH vibrations at around 3600-3000 cm^{-1}, γ CH and γ CH_2 vibrations (2898 cm^{-1} and 2871 cm^{-1}), δ CH_2 (sym) at C6 (1429 cm^{-1}), δ C-H (1371 cm^{-1}, 1282 cm^{-1}), δ COH in plane at C2 or C3 (1338 cm^{-1}), δ CH_2 (wagging) at C6 (1319 cm^{-1}), δ COH in plane at C6 (1236 cm^{-1} and 1202 cm^{-1}), as well as γ COC at β-glucosidic linkages (1165 cm^{-1}). Also observable are the γ ring in plane (1114 cm^{-1}), γ CO at C3 or γ C-C (1058 cm^{-1}), γ CO at C6 (1032 cm^{-1}, 1000 cm^{-1}), γ COC at β-glycosidic linkages, γ COC, γ CCO, and γ CCH at C5 and C6 (897 cm^{-1}), and δ COH out of plane (713 cm^{-1}, 668 cm^{-1}) vibrations (Figure 3.8, Table 3.2).

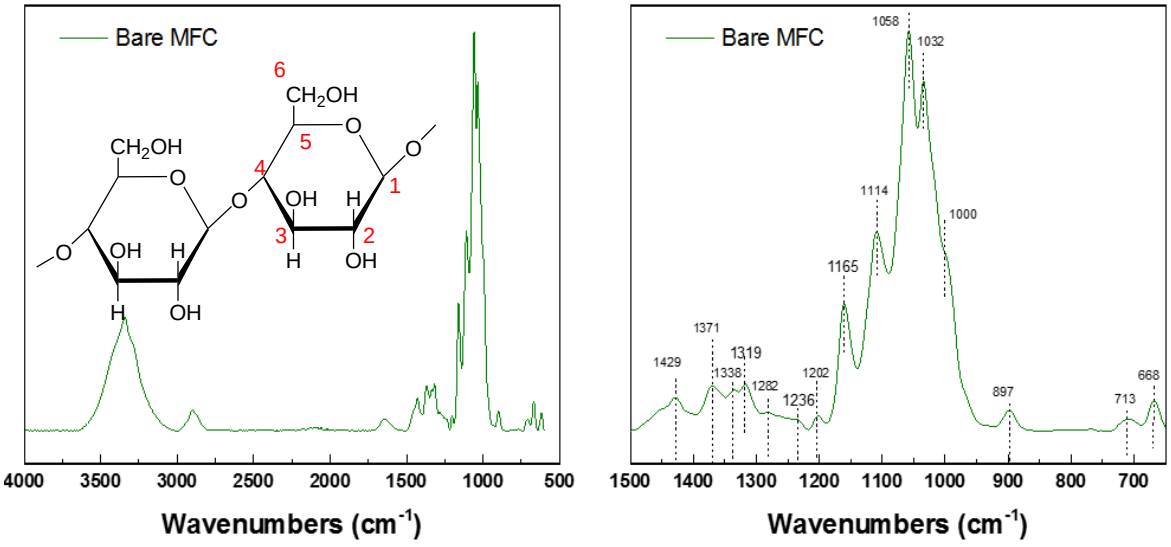

Figure 3.8. FTIR spectra of bare MFC and the monomer structure of cellulose.

Table 3.2. Vibrational assignments from FTIR spectra of bare, unfunctionalized MFC.

ν (cm^{-1})	Assignment δ:bending, γ stretching
~3000	γ OH (hydrogen bonding)
2901	γ CHn
1429	δ CH_2 (sym) at C6
1371	δ C–H
1338	δ COH in plane at C2 or C3
1319	δ CH_2 (wagging) at C6
1282	δ C–H
1236, 1202	δ COH in plane at C6
1165	γ COC at β-glucosidic linkage
1114	γ ring in plane
1058	γ CO at C3. γC–C
1032, 1000	γ CO at C6
897	γ COC at β-glycosidic linkage. γ COC, γ CCO, and γ CCH at C–5 and C–6
713	δ COH out of plane (cellulose Iβ)
668	δ COH out of plane

Figure 3.9 shows FTIR spectra for APDES modified MFC and bare MFC. Most of signature peaks of APDES are overlapping with signals from the MFC support because both materials consist of organic compounds. Each spectrum was normalized with the γ COC at β-glycosidic linkage peak (1165 cm^{-1}) for quantification purposes, because this peak is not affected by APDES and chemisorbed CO_2 species. Even though this FTIR analysis was conducted under ex-situ conditions such that the loss of OH groups due to grafting on the MFC could not be calculated because of bound water on adsorbents, the intensity of the other FTIR peaks of APDES increased as the silane loading increased on the MFC, as shown in Figure 3.9. Key bands include

δ NH_2 at 3346 cm^{-1} and 3290 cm^{-1} overlapped with γ OH vibrations of the MFC, γ CH_n at 2954, 2922, 2856 cm^{-1}, δ NH_2 at 1598 cm-1, γ Si-C at 1256 cm^{-1}, γ Si-OH, γ Si-O-C, γ Si-C(Asym), γ Si-O-Si (Asym), and γ Si-O-Si (Sym) between 1100 cm^{-1} and 762 cm^{-1} . These are signature peaks of APDES. Especially important are peaks at 1181 cm^{-1} and 1087 cm^{-1} are assigned to Si-O-cellulose linkages and these peaks of increasing intensity with APDES loading indicate that the hydrolyzed silanes were effectively grafted onto the MFC.

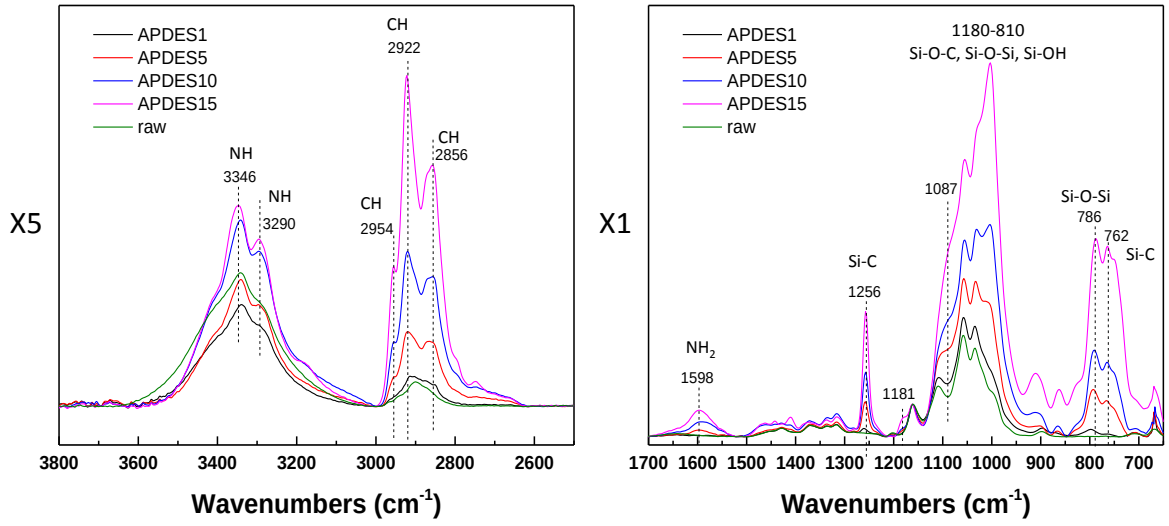

Figure 3.9. FTIR spectra of APDES modified MFCs as well asbare, unfunctionalized MFC

FTIR spectra of APTES modified MFC (Figure 3.10) are similar to those of APDES, including bands such as δ NH_2 at 3346, 1598 and 3290 cm^{-1}, γ CH_n at 2922 and 2856 cm^{-1}, as well as γ Si-OH, γ Si-C(Asym), γ Si-O-Si (Asym), γ Si-O-Si (Sym) peaks between 1100 cm^{-1} and 762 cm^{-1}. However, the γ Si-O-Si signal at 1143 cm^{-1}, a distinguishing peak compared with the APDES/MFC samples, is quite noticeable. This peak corresponds to poly(siloxane)s made up of T mode species. As shown in Figure 3.7, APTES hydrolyzed and condensed into a three way

network and consequently formed a bulk 3D structure, which was also supported by FTIR spectra. On top of that, the γ Si-C vibration (Si-CH_3) at 1256 cm^{-1} for APDES was not observed from the APTES samples, because APTES contains only three alkoxy groups, with no methyl group (-CH_3) connected to the Si of APTES. Thus, Si-O-Cellulose linkage peaks were not noticeable for APTES/MFC samples, which can be interpreted as suggesting that most of the hydrolyzed APTES primarily condensed with other silane species instead of being grafted on the MFC. Since the condensed APDES structure is similar to the linear cellulose fiber, they could be easily stacked with each other. However, in the case of the condensed APTES, the hydroxyl group of the cellulose fibers would not easily interact with 3D APTES poly(siloxane) structure because of steric hindrance. Consequently, the relative density of Si-O-cellulose peaks for APDES/MFC appeared higher than for the APTES/MFC material.

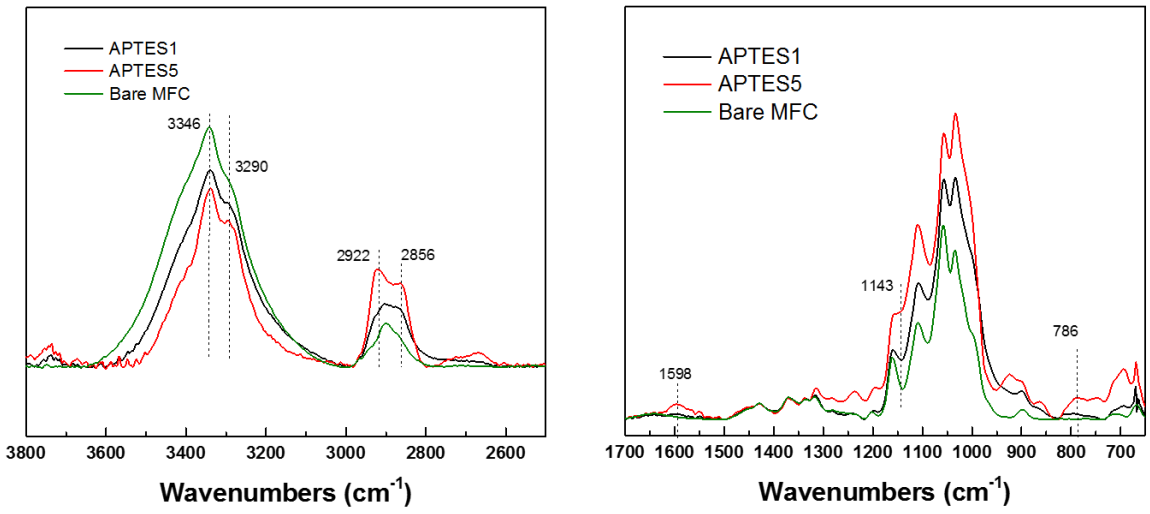

Figure 3.10. FTIR spectra of APTES modified MFCs and bare, ungrafted MFC.

In-situ CO_2 adsorption FTIR spectra of APDES modified MFC

The chemisorbed CO_2 species on APDES modified MFCs were verified with in situ FTIR spectroscopy. In the case of numerous FTIR studies with inorganic adsorbents, chemisorbed CO_2 species appear in a range (1800 cm^{-1} - 1200 cm^{-1}) that does not overlap much with the signals of the adsorbent, and thus, the chemisorbed CO_2 species could be easily observed. However, it was not easy to verify the nature of the adsorbed species (carbamate vs. carbamic acid) on the amine functionalized MFC, because some of the IR peaks of organic moieties for cellulose overlap with these species. Furthermore, since the intensity of chemisorbed CO_2 species are not remarkable compared to the IR peak of cellulose, formed species are not easily distinguished. Once the MFC adsorbents are exposed to air, it adsorbed water as well as CO_2, which could affect the nature of the chemisorbed CO_2 species. For these reasons, ex-situ IR studies for CO_2 chemisorbed species on amine-modified cellulose have shown limited information. To facilitate the IR studies, an amine functionalized MFC material was synthesized as a film instead of via freeze drying, and 10 mbar of CO_2 was injected over the film in an IR in-situ cell. As the CO_2 exposure time increased, the intensity of the IR bands for adsorbed CO_2 also increased, which indicated that the APDES modified MFC film could adsorb CO_2. As shown in Figure 3.11, alkyl ammonium carbamate ion pairs were observed at 1631 cm^{-1}, 1575 cm^{-1}, 1483 cm^{-1}, 1431 cm^{-1}, 1382 cm^{-1}, 1323 cm^{-1}. Didas et al.[16] reported similar FTIR spectra for highly APTMS loaded (4.33 nmmol/g) SBA15 silica adsorbent under dry CO_2 adsorption conditions, and carbamic acid and silylpropylcarbamate species were also observed at low APTMS loadings (1.65 N mmol/g).This was interpreted as suggesting that metastable carbamic acid species were stabilized by silanols via hydrogen bonding and silylpropylcarbamate species were formed from this carbamic acid via water condensation, as suggested by Bacsik et al.[17] However, due to the high APDES loading (5 N mmol/g) on the MFC

sample used for the IR study here, only alkyl ammonium carbamate species were observed, while cabamic acid or silylpropyl carbamate species were not observed. This suggests that the hydroxyl groups of MFC were occupied by other hydroxyl groups via hydrogen bonding or were removed by the silane grafting.

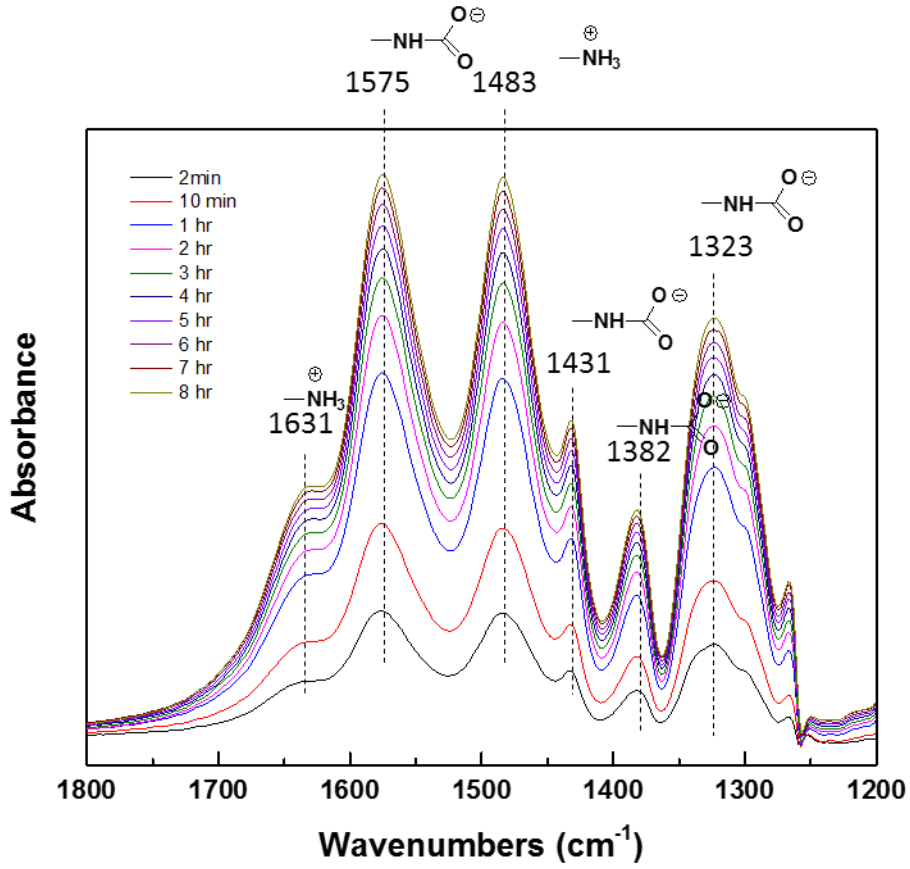

Figure 3.11. In-situ FTIR spectra of CO_2 adsorption on an APDES 10 film.

3.4. Conclusions

3.4.1. CO_2 adsorption for amine impregnated MFC (Class 1)

TREN and PEI molecules were impregnated into MFC supports, and the propensity for CO_2 adsorption was compared with TREN and PEI modified SBA15 adsorbents. Even though the CO_2 uptake rate (kinetics) of MFC based adsorbents were relatively slower than silica based

adsorbents, considering their limited surface area (25 m^2/g) and pore volume (0.05 cm^3/g), competitive CO_2 uptakes and amine efficiencies were observed from PEI/MFCs. However, the TREN40/MFC material did not adsorb CO_2 while the TREN40/SBA15 could adsorb 0.6 mmol CO_2/g with 400 ppm CO_2 flowing over it for 500 min. From the TGA analysis of TREN impregnated adsorbents and pure TREN, it was suggested that TREN could evaporate at the pretreatment temperature (120 ^oC) used for CO_2 adsorption because of the high volatility of TREN, even though it has high boiling point (265 ^oC). A highly thickened fiber diameter (30 μm) of TREN40/MFC was observed from SEM images while the diameter of fibers for PEI40/MFC only slightly increased compared to the bare MFC. Hypothetically, the primary amines of TREN might interact with the hydroxyl groups of MFC via hydrogen bonding, and TREN could act as a binder between adjacent MFC fibers and consequently, TREN-embedded thick cellulose fiber were formed after freeze drying. In contrast, PEI thickened the fibers much less, likely due to the bulky nature of the branched PEI, which may have acted as a cellulose spacer.

3.4.2 CO_2 adsorption for organosilane modified MFC (Class 2)

Various amount of APDES or APTES were grafted on MFCs and their CO_2 uptakes were measured. There were noticeable differences in CO_2 uptake between APDES and APTES modified MFC. While the CO_2 uptake for APDES/MFC increased with APDES loading, APTES/MFC showed very low CO_2 uptakes, with even high APTES loadings. By increasing the APDES loadings on the MFC support, a sheet structure was developed, with poly(siloxane) filling the void area. However, after the sheet structure was developed at low APTES loadings, no significant morphology changes were observed. Instead of filling void area with the sheet structure, bulk condensed APTES polysiloxanes were observed. From the solid state ^{29}Si NMR and ex-situ FTIR

analysis of APDES or APTES modified MFCs, their poly(siloxane) structures were inferred and Si-O-Cellulose linkages were observed from only APDES/MFC. Chemisorbed CO_2 species (alkyl ammonium carbamate) from APDES10 were detected with in-situ FTIR analysis under dry CO_2 adsorption conditions. From this study, the differences in the structure of APDES and APTES modified MFCs showed key evidence for why the APDES material had remarkably enhanced CO_2 adsorption capacities.

3.5. References

(1) Harlick, P. J. E.; Sayari, A. Applications of Pore-Expanded Mesoporous Silicas. 3. Triamine Silane Grafting for Enhanced CO2 Adsorption. *Ind. Eng. Chem. Res.* **2006**, *45* (9), 3248–3255.

(2) Gebald, C.; Wurzbacher, J. A.; Tingaut, P.; Zimmermann, T.; Steinfeld, A. Amine-Based Nanofibrillated Cellulose As Adsorbent for CO2 Capture from Air. *Environ. Sci. Technol.* **2011**, *45* (20), 9101–9108.

(3) Wurzbacher, J. A.; Gebald, C.; Steinfeld, A. Separation of CO2 from Air by Temperature-Vacuum Swing Adsorption Using Diamine-Functionalized Silica Gel. *Energy Environ. Sci.* **2011**, *4* (9), 3584.

(4) Gebald, C.; Wurzbacher, J. a.; Borgschulte, A.; Zimmermann, T.; Steinfeld, A. Single-Component and Binary CO2 and H2O Adsorption of Amine-Functionalized Cellulose. *Environ. Sci. Technol.* **2014**, *48* (4), 2497–2504.

(5) Gebald, C.; Wurzbacher, J. a.; Tingaut, P.; Steinfeld, A. Stability of Amine-Functionalized Cellulose during Temperature-Vacuum-Swing Cycling for CO2 Capture from Air. *Environ. Sci. Technol.* **2013**, *47* (17), 10063–10070.

(6) Wang, B.; Sain, M. Dispersion of Soybean Stock-Based Nanofiber in a Plastic Matrix. *Polym. Int.* **2007**, *56* (4), 538–546.

(7) Cheng, Q.; Wang, S.; Rials, T.; Lee, S.-H. Physical and Mechanical Properties of Polyvinyl Alcohol and Polypropylene Composite Materials Reinforced with Fibril Aggregates Isolated from Regenerated Cellulose Fibers. *Cellulose* **2007**, *14* (6), 593–602.

(8) Okubo, K.; Fujii, T.; Thostenson, E. T. Multi-Scale Hybrid Biocomposite: Processing and Mechanical Characterization of Bamboo Fiber Reinforced PLA with Microfibrillated Cellulose. *Compos. Part A Appl. Sci. Manuf.* **2009**, *40* (4), 469–475.

(9) Auad, M. L.; Contos, V. S.; Nutt, S.; Aranguren, M. I.; Marcovich, N. E. Characterization of Nanocellulose- Reinforced Shape Memory Polyurethanes. *Polym. Int.* **2008**, *57* (4), 651–659.

(10) Fernández, A.; Sánchez, M. D.; Ankerfors, M.; Lagaron, J. M. Effects of Ionizing Radiation in Ethylene-Vinyl Alcohol Copolymers and in Composites Containing Microfibrillated Cellulose. *J. Appl. Polym. Sci.* **2008**, *109* (1), 126–134.

(11) Klemm, D.; Heublein, B.; Fink, H.-P.; Bohn, A. Cellulose: Fascinating Biopolymer and Sustainable Raw Material. *Angew. Chemie Int. Ed.* **2005**, *44* (22), 3358–3393.

(12) Bel-Hassen, R.; Boufi, S.; Salon, M.-C. B.; Abdelmouleh, M.; Belgacem, M. N. Adsorption of Silane onto Cellulose Fibers. II. The Effect of pH on Silane Hydrolysis, Condensation, and Adsorption Behavior. *J. Appl. Polym. Sci.* **2008**, *108* (3), 1958–1968.

(13) Savard, S.; Blanchard, L.-P.; Léonard, J.; Prud'homme, R. E. Hydrolysis and Condensation of Silanes in Aqueous Solutions. *Polym. Compos.* **1984**, *5* (4), 242–249.

(14) Brochier Salon, M.-C.; Abdelmouleh, M.; Boufi, S.; Belgacem, M. N.; Gandini, A. Silane Adsorption onto Cellulose Fibers: Hydrolysis and Condensation Reactions. *J. Colloid Interface Sci.* **2005**, *289* (1), 249–261.

(15) Abdelmouleh, M.; Boufi, S.; Belgacem, M. N.; Dufresne, A.; Gandini, A. Modification of Cellulose Fibers with Functionalized Silanes: Effect of the Fiber Treatment on the Mechanical Performances of Cellulose-Thermoset Composites. *J. Appl. Polym. Sci.* **2005**, *98* (3), 974–984.

(16) Didas, S. A.; Sakwa-novak, M. A.; Foo, G. S.; Sievers, C.; Jones, C. W. Effect of Amine Surface Coverage on the Co-Adsorption of CO2 and Water: Spectral Deconvolution of Adsorbed Species. *J. Phys. Chem. Lett.* **2014**, *5*, 4194−4200.

(17) Bacsik, Z.; Ahlsten, N.; Ziadi, A.; Zhao, G.; Garcia-Bennett, A. E.; Martín-Matute, B.; Hedin, N. Mechanisms and Kinetics for Sorption of CO 2 on Bicontinuous Mesoporous Silica Modified with N-Propylamine. *Langmuir* **2011**, *27* (17), 11118–11128.

CHAPTER 4

SUMMARY

For effective control of the increasing atmospheric CO_2 concentration, development of direct CO_2 capture technologies from air is necessary, for use in parallel with flue gas capture processes at point sources. Since DAC requires a massive amount of air flow because of diluted CO_2 concentration of air, a low pressure drop CO_2 capture system with amine containing solid adsorbents may be suitable because low pressure drops can be achieved with high CO_2 uptakes. To this end, numerous DAC studies have been conducted with these amine containing adsorbents but only a few have focused on elucidating the molecular level aspects of CO_2 adsorption with amines. From the study presented in chapter 2, CO_2 adsorption via intramolecular vs. intermolecular amine interactions was explored by focusing on silica materials with ultra-low silane loadings. Cooperative amine interactions with silanols were verified by capping silanols with HMDS and observing the changes in CO_2 adsorption behavior. In addition, the hypothesis that intramolecular sorption can occur on a single silane chain that contains multiple amines was supported by this array of experiments. Simultaneously the heats of adsorption from the intramolecular interactions were measured and the evolved heats were assigned to probable CO_2 adsorption pairs.

With this new understanding of amine interactions on solid adsorbents, the potential for use of a new support material, MFC, was evaluated and the results are described in chapter 3. From the structural morphologies and CO_2 uptakes for PEI or TREN impregnated MFC adsorbents, it was inferred that TREN might be intercalated between MFC fibers via hydrogen bonds between the primary amines of TREN and hydroxyl groups of MFC. Thus the diameters of TREN40/MFC

fibers were thickened up to 30 μm and the CO_2 uptake for the TREN40/MFC material was very low. On the other hand, the branched structure of PEI was assumed to provide space between the fibers and consequently, the CO_2 uptake for PEI40/MFC was good, being only slightly lower than for PEI40/SBA15. As an application of MFC for class 2 materials, organosilanes containing different numbers of alkoxy groups were grafted on MFC. It was noteworthy that the APDES modified MFC adsorbent showed a remarkable CO_2 uptake but the APTES modified MFC adsorbent showed poor CO_2 uptake. From the FTIR, solid state ^{29}Si NMR and SEM analyses, it was verified that APDES grafted MFC had a linear structure while APTES modified MFC contained locally lumped poly(siloxane)s. Thus, amine molecules seemed not to be uniformly dispersed as in APDES/MFC, which was hypothesized to contribute to the low CO_2 uptake. From these studies, it can be concluded that MFC is a support material with acceptable utility for CO_2 adsorption but additional studies need to be conducted to understand the basis for the high CO_2 uptake even though the MFC has limited surface area and pore volume.